JOURNAL OF GEOPHYSICAL RESEARCH, VOL. 103, NO. A11, PAGES 26,197–26,220, NOVEMBER 1, 1998

An overview of the early November 1993 geomagnetic storm

D. J. Knipp,[1] B. A. Emery,[2] M. Engebretson,[3] X. Li,[4] A. H. McAllister,[2] T. Mukai,[5] S. Kokubun,[6] G. D. Reeves,[7] D. Evans,[8] T. Obara,[9] X. Pi,[10] T. Rosenberg,[11] A. Weatherwax,[11] M. G. McHarg,[1] F. Chun,[1] K. Mosely,[1] M. Codrescu,[8] L. Lanzerotti,[12] F. J. Rich,[13] J. Sharber,[14] and P. Wilkinson[15]

Abstract. This paper describes the development of a major space storm during November 2-11, 1993. We discuss the history of the contributing high-speed stream, the powerful combination of solar wind transients and a corotating interaction region which initiated the storm, the high-speed flow which prolonged the storm and the near-Earth manifestations of the storm. The 8-day storm period was unusually long; the result of a high-speed stream (maximum speed 800 km/s) emanating from a distended coronal hole. Storm onset was accompanied by a compression of the entire dayside magnetopause to within geosynchronous Earth orbit (GEO). For nearly 12 hours the near-Earth environment was in a state of tumult. A super-dense plasma sheet was observed at GEO, and severe spacecraft charging was reported. The effects of electrons precipitating into the atmosphere penetrated into the stratosphere. Subauroral electron content varied by 100% and *F* layer heights oscillated by 200 km. Equatorial plasma irregularities extended in plumes to heights of 1400 km. Later, energetic particle fluxes at GEO recovered and rose by more than an order of magnitude. A satellite anomaly was reported during the interval of high energetic electron flux. Model results indicate an upper atmospheric temperature increase of 200°K within 24 hours of storm onset. Joule heating for the first 24 hours of the storm was more than 3 times that for typical active geomagnetic conditions. We estimate that total global ionospheric heating for the full storm interval was ~190 PJ, with 30% of that generated within 24 hours of storm onset.

1. Introduction

This paper presents a synthesis of the space environment for the interval November 2-11, 1993. We briefly discuss the geomagnetic activity in late 1993 and then develop a synopsis of the indices available for global storm assessment, investigate the solar wind interaction with the near-Earth environment, and describe, in detail, the impacts and observations associated with this major space weather disturbance. In sequence, we deal with observations associated primarily with storm onset and then with observations from the full storm interval. Energetic electrons and the storm energy budget are discussed in separate sections. We present the data and model output profiles in a common time line format. The general paradigms for our analysis come from reviews by *Akasofu* [1981], *Gonzalez et al.* [1994], *Buonsanto and Fuller-Rowell* [1997], and *Prölss* [1997].

The overall study combines data sets from Yohkoh, Geostationary Operational Environmental Satellite 7 (GOES 7), Interplanetary Monitoring Platform 8 (IMP 8), and Geotail satellites to investigate the solar and solar wind origin of the storm. Observations from up to seven geostationary Earth orbiting (GEO) satellites helped establish the state of the inner magnetosphere and plasmasphere and, for a few crucial moments, the location of the magnetopause. During the storm, continuous data were recorded by over 150 ground magnetometer stations, nine low Earth orbit (LEO) satellites, three coherent backscatter Super Dual Auroral Network (SuperDARN) radars, and numerous ionosondes, digisondes, riometers, and ground Global Positioning Satellite (GPS) receiver sites. Occasional and intermittent observations were available from three incoherent backscatter radars, an ionospheric tomography chain, and high-latitude photometers. Data were acquired from all of the World Data Centers and several university and international archives. At least ten major models or data assimilation procedures contributed. The combined interplanetary data sets show small-scale transients embedded within the corotating interaction regions (CIR) between two solar wind streams. The storm data, discussed in sections 3–5, show that the superposition of

[1] Department of Physics, U.S. Air Force Academy, Colorado.
[2] High Altitude Observatory, National Center for Atmospheric Research, Boulder, Colorado.
[3] Department of Physics, Augsburg College, Minnesota.
[4] Laboratory for Atmospheric and Space Physics, University of Colorado, Boulder, Colorado.
[5] Institute for Space and Astronautical Science, Sagamihara, Japan.
[6] Solar Terrestrial Environment Laboratory, Toyokawa, Japan.
[7] Los Alamos National Laboratory, Los Alamos, New Mexico.
[8] Space Environment Center, National Oceanic and Atmospheric Administration, Boulder, Colorado.
[9] Hiraiso Solar Terrestrial Research Center, Ibaraki, Japan.
[10] Jet Propulsion Laboratory, California Institute of Technology, Pasadena.
[11] Institute for Physical Science and Technology, University of Maryland, College Park.
[12] Bell Laboratories, Lucent Technology, Murray Hill, New Jersey.
[13] Space Vehicles Directorate, Air Force Research Laboratory, Hanscom AFB, Massachusetts.
[14] Southwest Research Institute, San Antonio, Texas.
[15] IPS Radio and Space Services, Haymarket, New South Wales, Australia.

Paper number 98JA00762.
0148-0227/98/98JA-00762$09.00

transients and high density CIR had striking effects on the near-Earth environment. The data also indicate that Alfvenic fluctuations in the trailing high-speed stream served to enhance and prolong the storm.

One of the most significant challenges in the realm of understanding magnetospheric storms is the diagnosis and forecasting of energetic electron behavior. The 27-day periodicity of energetic electron enhancement has been known for over 3 decades [*Williams*, 1966], and for nearly 2 decades the association between enhancements and high-speed streams has been recognized [*Paulikas and Blake*, 1979]. *Li et al.* [1997] establish a close association between the moderate to intense geomagnetic storms of late 1993 and periodic enhanments of high-energy electrons. However, energetic electron behavior remains enigmatic. *Baker et al.* [1997] report flux enhancements occur even during relatively weak geomagnetic activity. Flux enhancements generally follow storm onset within 48-72 hours, but during some storms the flux rise is preceded by a notable drop-out of high-energy electrons [*Baker et al.*, 1994; *Korth and Friedel*, 1997]. The cessation of high-energy electron flux events can be abrupt. *Reeves* [1998] finds only a weak correlation between *Dst* and intensity of the recovery phase 0.5 – 7.8 MeV electron enhancement, yet, in a survey of 25 storms, *Nakamura et al.* [this issue] find a strong correlation between intensity of the 1 MeV flux drop-outs at storm onset and the intensity of the storm as measured by the *Dst* index. In sections 2 and 5 we discuss the data for this storm and the related studies which address the following questions: "Where do the electrons go at storm onset?" "How are they replenished?" and "Why are some variations rhythmic and some aperiodic?"

Recent numerical simulations have yielded insight into global and seasonal ionospheric response [*Fuller-Rowell et al.*, 1996; 1997], but synoptic and local diagnosis and prediction of ionospheric storm features continue to challenge the scientific community. *Codrescu et al.* [1997a] point out that while global response tends to be linear with respect to energy input, regional and local responses are highly nonlinear due to combined effects of dynamics, chemistry, and auroral forcing. Spatial and temporal variations, especially for Joule heating, are of significant physical consequence since explosive or prolonged Joule heating drives auroral wind surges that propagate globally. The propagation moves plasma, changes total electron content (TEC), and alters chemical composition producing a positive ionospheric storm phase (increased ionization) [e.g., *Buonsanto and Fuller Rowell*, 1997]. They note that chemical composition "bulges" created during stormtime can be further redistributed by background and storm wind fields, thus creating additional feedback loops which give rise to ionospheric negative storm phase (decreased ionization). In section 6 we provide estimates of the overall ionospheric energy budget for the storm and a discussion of the high-latitude ionospheric variations.

2. Background

The event is one example of the particularly strong recurrent storms of the declining phase of solar cycle 22. The propensity for strong storms in the declining phase of even-numbered solar cycles has been documented by *Cliver et al.* [1996] and *Crooker et al.* [1996]. The former study found a prominent 27-day recurrence pattern related to rapid expansion of polar coronal holes at the end of every other 11-year Hale cycle. The latter study noted that the seasonal heliographic latitude [*Rosenberg and Coleman*, 1969] effect and the seasonal interplanetary field projection effect [*Russell and McPherron*, 1973] can combine to strengthen geomagnetic activity. Thus there is equinoctial access to, and prolonged immersion in unusually high speed flow, and exposure to interplanetary magnetic field (IMF) sector polarities (away in the autumn) that favor enhanced geomagnetic activity in the declining phase of the even numbered solar cycles. Such influences appeared in late 1993.

In mid-1993 the solar corona underwent a significant restructuring; shifting from a four-sector structure to a two-sector structure [*Watari*, 1995] with a single coronal hole extension to low latitudes [*Crooker and McAllister*, 1997]. Yohkoh soft Xray images revealed a long-lived coronal hole recurrently present from August through December 1993. During early November 1993 (fourth recurrence), the northern polar hole extended across the nominal solar equator [*McAllister et al.*, this issue; C.-C. Wu et al., unpublished manuscript] and reached its maximum longitudinal extent [*Knipp and Emery*, 1998]. It is this fourth recurrence that is the primary subject of this paper, but in an effort to put the November storm in context, we next present information about the associated storm series as it developed in late 1993.

Beginning in August, strong geomagnetic activity fell into a 27-day recurrent storming cycle. The activity became so cyclical that campaigns for studying ionospheric storm effects were planned and executed for the storm we discuss here. Various observing groups were operating in special mode to take advantage of the anticipated storm conditions [*Foster et al.*, 1994a; *Bust et al.*, 1997; *Foster et al.*, this issue]. Although storm timing was predictable to a degree, forecasting the level of activity proved to be quite problematic for all of the recurrent events in this series. (J. Kunches, personal communication, 1996). *Crooker and McAllister* [1997] and *McAllister and Crooker* [1997] argue that the recurrent storms were actually a combination of transient and corotating disturbances, thus introducing an element of randomness to the strength of the each recurrence. They found considerable evidence for the enhancements of geo-effectiveness of recurrent storms by "transient" activity, noting that from August 1993 to May 1994, the Sun released transients from a number of active regions bordering the low latitude extension of the north polar coronal hole and from the southern crown. Many of these releases were at the base of the heliospheric current sheet, allowing for Earth arrival of transients close to the CIR.

Strong storming was also influenced by Alfvenic IMF fluctuations typical of high-speed streams [*Gonzalez and Tsurutani*, 1987] and by IMF sector polarity. *McAllister and Crooker* [1997] point out that the late 1993 north polar coronal hole extension responsible for the dominant high-speed stream had an IMF "away" (B_x negative, B_y positive) orientation. Autumn passage of away polarity enhances merging owing to the Russell-McPherron effect.

Prior to this study a coherent picture of the late 1993 solar wind record did not exist. We have assembled a variety of data to remedy the situation. Figure 1 shows a composite of indices and observations for the latter half of 1993. On the basis of the 27-day recurrence pattern in the geomagnetic indices and observations (Figures 1d-1j), and the solar wind speed and ultralow frequency (ULF) wave data, we draw vertical lines to highlight the recurrence of the solar wind stream responsible for the November 1993 storm. This stream was

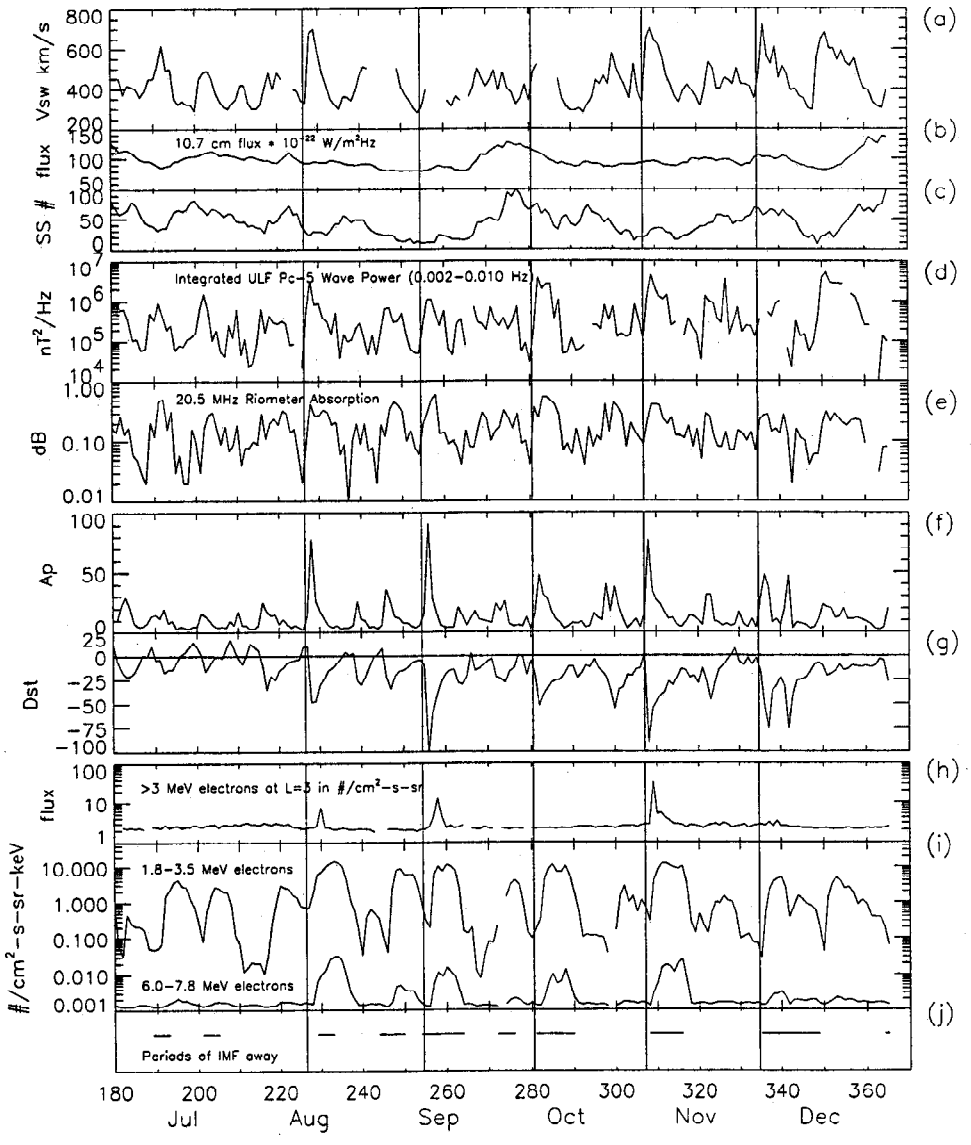

Figure 1. (a) Solar wind speed measured by Geotail (top curve) for daily intervals between 0600 and 0800 UT, (b) F10.7 cm flux, (c) sunspot number, (d) integrated ultralow frequency wave power in 2-10 mHz band for the daily intervals between 0600 and 0800 UT, (e) the daily average 20.5 MHz riometer absorption measured at South Pole Station, (f) the *Ap* index, (g) the daily average *Dst* index, (h) the daily integrated flux of > 3 MeV electrons at L=3, (i) the daily differential flux of 1.8-3.5 MeV electrons and 6.0-7.8 MeV electrons at L=6.6. (j) indicators of the IMF "away" sector. All data cover the interval from days 180-365 of 1993.

associated with a series of storms that we refer to as the "primary series." Figures 1b and 1c show the signatures of the declining phase of solar cycle 22: relatively low sunspot number (< 100) and a *F*10.7 cm flux values near 100 flux units. Figure 1a combines partial-day observations (~6-hour averages) of solar wind speed from IMP 8 and Geotail satellites. Many of the observations were made by Geotail in the distant magnetosheath, where mixing allowed reasonable penetration of the bulk solar wind flow [*Nakamura et al.*, 1997]. The speed record is incomplete because of transits of the spacecraft into the magnetosphere.

In Figure 1, there is ample evidence of recurrent high-speed streams. *Engebretson et al.* [this issue], combined records of solar wind and integrated ULF Pc5 wave power at cusp and auroral zone stations, to demonstrate two high-speed streams within the interval. The ULF record from Cape Dorset, Canada, a nominal cusp station at 74.5° magnetic latitude (MLAT), is shown in Figure 1d. It presents the power between 2 and 10 mHz calculated using 1-hour FFT intervals, averaged over all local times between 0800 and 1400 MLT. The steep rises in ULF power at days 254 and 282 give a good indication that the leading edge of high-speed streams passed the earth. The lack of a rise at day 336 (last storm in the primary series) is due to a data gap. Data from a lower-latitude station show a short-lived increase in ULF power on that day. Data in Figure 1 suggest organization of the primary high-speed stream as early as day 200, but that stream passage did not produce a major storm. Subsequently, the stream produced major or moderate storms in five sequential 27-day Carrington solar rotations; a duration consistent with

the findings of *Mursula and Zieger* [1996] who note that "activations" of two-stream structures have an average lifetime of about four Carrington rotations.

Although the primary series did not include the strongest storm of 1993, the series consistently yielded storms with effects throughout the Earth's magnetic domain. *Kokubun et al.* [1996] provide a list of events for which large magnetotail field lobe values were observed by the Geotail spacecraft. Of the 24 events listed for the interval late-1992 to late-1994, four are from the primary storm series. The August through November recurrences produced lobe field values three or more times the typical value of 9 nT.

Additional responses to the recurrent and transient forcing are illustrated in Figures 1e-1j. Figure 1e shows the daily average relative ionospheric opacity measurements (riometer) absorption (20.5-MHz band) data from South Pole Station, Antarctica. The riometer technique is based on absorption of cosmic radio noise [*Detrick and Rosenberg*, 1990] which is often caused by energetic electron precipitation (> 10 keV) increasing the electron density in the *D* and *E* regions of the ionosphere. *Weatherwax et al.* [1997] noted that substorm-related precipitation at these very high latitudes has a tendency to be associated with high-speed streams. Daytime absorption occurs when the station rotates under the dayside auroral zone. Nightside absorption occurs as the result of expansion of substorm electron precipitation into the polar cap. Daily averages are sensitive to both temporal and spatial expansion of auroral zone activity. The absorption profile and the profile of ULF Pc5 wave power show strong correlation. The correlation appears to grow stronger after mid-August, suggesting that both sets of observations are strongly modulated by high-speed streams.

The *Ap* index is plotted in Figure 1f. The five largest values of *Ap* in late 1993 were associated, one each, with the primary series storms. Three of the five recurrences registered as major storms with $Ap > 50$. The November recurrence was the second strongest in the series. Figure 1g shows the daily averaged *Dst* values. The strongest *Dst* storms in the latter half of 1993 occurred with the September, November, and December appearances of the primary high-speed stream.

In late 1993, energetic electron fluxes were repeatedly enhanced in the inner magnetosphere [*Li et al.*, 1997]. Figure 1h shows the daily values of the integral flux of ≥ 3 MeV electrons measured by the Solar Anomalous and Magnetospheric Particle Explorer (SAMPEX) satellite at L=3. From these data sets we observe that three of the primary series storms were especially effective enhancing the L=3 population. The enhanced fluxes at L=3 are associated only with the primary series and in particular, with those recurrences generating peak *Ap* values. Figure 1i shows the history of the differential flux of 1.8-3.0 MeV (nominally ≥ 2 MeV) electrons (top curve) and ≥ 6 MeV electrons (bottom curve) at GEO for late 1993. The observations were made by the energetic spectrometer for particles (ESP) instrument on the Los Alamos National Laboratory (LANL) satellite 1989-046. Figure 1j shows bars from a somewhat incomplete data set that indicates when the IMF polarity was in the "away" sector. The data coverage is poor for days 180-230 and better, but still intermittent, for days thereafter. Despite the limited coverage, we see a tendency for energetic electron activation with onset of the IMF away polarity, a polarity known to enhance geomagnetic activity during the northern hemisphere autumn months.

3. Early November 1993 Storm

3.1. Global Composite Indices

By nearly all accounts the November 2-11, 1993 storm was a "major" storm. The storm ranked in the top 25% of the major magnetic storms recorded since 1932 using the 24-hour *Ap** criteria (J. Allen, http://www.ngdc.gov/stp/ GEOMAG/ apstar.html) and it met the major storm threshold of hourly $Dst < -100$ nT [*Rostoker et al.*, 1980] and also the *Gonzalez and Tsurutani* [1987] criteria for an intense storm: $Dst < -100$ nT and $B_z < -10$ nT for more than 3 hours. November 4, 1993, was designated the most disturbed day of the month based on an *Ap* value of 77 (Solar Geophysical Data Prompt Reports, no. 593, part 1, 1994). There is no single agreed upon way to gauge storm intensity. In Figure 2, we present a group of indices that allows relevant comparisons among most interested investigators. In later figures, we present additional useful measures of storm intensity.

The *Kp*, *ap*, and *Ap* indices are shown in Figures 2a and 2b. During most of November 2-3, the indices indicated unusual geomagnetic quiescence. Activity levels exceeding alert criteria ($Kp \geq 5$) [*Joselyn*, 1995] developed late on November 3 and extended through November 4. Severe storm limits in the *ap* index were exceeded between 0000 and 0300 UT, November 4, and major storm threshold was exceeded most of that day. By *Ap* thresholds [*Joselyn*, 1995], November 2 and 3 were geomagnetically quiet, while November 4 was a major storm day. November 5-7 were active days, and November 8-11 were unsettled days.

Figure 2c shows a 15-min resolution, high-latitude storm perspective using the polar cap (PC) index. The index was developed by *Troshichev et al.* [1988], and further elucidated by *Vennerstrøm et al.* [1991], to characterize the degree of solar wind coupling with the magnetosphere. It is derived from ground magnetometer observations in one or both polar caps (in this case the index is derived from Thule, Greenland). The index was formulated so that values ≥ 1 are closely associated with southward IMF [*Troshichev et al.*, 1996]. Probability distributions for the Thule PC index (1979 to 1995) show that values of 4 or greater occur less than 7% of the time in the Thule data, while values of 7 or greater occur less than 3% of the time.

At ~1800 UT, November 3, there was an undulation in the IMF Bz component (Figure 4g). The PC index rose to a value of 3. Late on November 3, in response to extremely effective coupling conditions in the solar wind, the PC values exceeded 7. On November 4, the average PC index value exceeded 4 with the highest values recorded during passage of the CIR. This was the highest PC index daily average of late 1993. Strong solar wind-magnetosphere interaction continued in the presence of Alfvenic fluctuations through November 7 but slowly decreased thereafter. Well-separated substorms are evident in the PC index record on November 9-11. High-latitude convection patterns derived from data assimilation indicate that the extreme PC value on November 8 was associated with a major high-latitude convection reconfiguration and substorm.

The level of activity in and around the auroral zone was similarly high. The extent of the auroral zone can be moni-

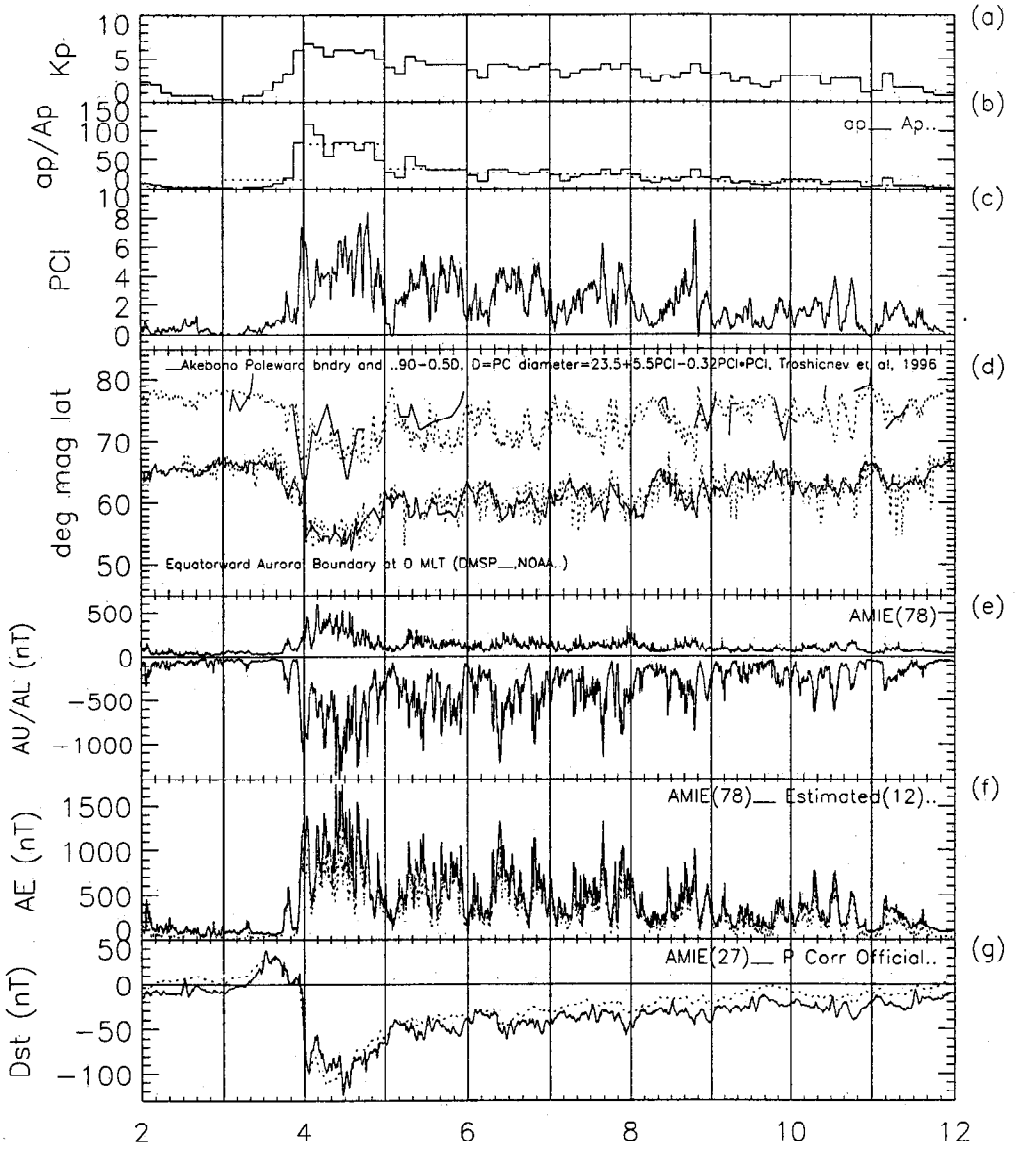

Figure 2. (a) The *Kp* index, (b) The *ap* index (solid curve) and the *Ap* index (dashed curve), (c) the polar cap index, (d) an estimate of the poleward boundary of the aurora (top dotted curve), observations of the poleward boundary from the Akebono satellite (top solid curve), estimates of the midnight equatorward boundary of the aurora from DMSP (solid) and NOAA 12 (dashed), (e) the *AU* index estimated from 78 stations (top) and the *AL* index estimated from 78 stations (lower), (f) the *AE* index estimated from 78 stations (solid) and estimated from the 12 official AE stations (dashed), (e) the *Dst* index estimated from 27 stations (solid) and the pressure-corrected *Dst* from official stations (dashed). All data are for November 2-11, 1993.

tored with the auroral boundary index (*ABI*) and to some degree with the PC index. The *ABI*, available from the U. S. Air Force Research Laboratory, estimates the latitude of the midnight equatorward boundary of the auroral zone based on Defense Meteorological Satellite Program (DMSP) observations of the diffuse aurora from polar passes over both auroral zones [*Gussenhoven et al.*, 1983]. A similar algorithm has been developed for the NOAA TIROS satellite data. In Figure 2d, the lower solid curve shows the *ABI* estimates made roughly every 30 min from three DMSP satellites. The bottom dashed curve shows the NOAA 12 estimate of the equatorward boundary. The orbit for NOAA 12 was less conducive to such estimates; hence there is more scatter in the NOAA equatorward boundary location. The upper curve in Figure 2d is an estimate of the dawn and dusk poleward boundaries of the auroral zone. The estimates are derived from the PC index, based on a formula from *Troshichev et al.* [1996], who compared poleward boundary estimates from the Akebono satellite to the PC index. Observations of the southern hemisphere dawn and dusk poleward boundaries made by the Akebono satellite for this event are superposed on the upper curve in Figure 2d.

Both boundaries of the auroral zone were contracted to high latitudes for the interval 1800 UT, November 2 to 1800 UT, November 3, as expected with the low geomagnetic activity level [*Feldstein and Starkov*, 1967]. An expansion to more typical latitudes began at about 1800 UT, November 3, consistent with the southward IMF turning observed by both

IMP 8 and Geotail satellites. For a short time after main phase onset (2300 UT, November 3) Akebono observed a very thin dawn and dusk auroral zone as the poleward boundary expanded equatorward, but the equatorward boundary remained at relatively high latitudes. The rapid, equatorward expansion of the auroral zone to 55° MLAT just after 0000 UT, November 4, was recorded by all satellites at a variety of local times indicating a global auroral response of significant magnitude. Data from the Upper Atmospheric Research Satellite (UARS) during the interval 0800-0930 UT, November 4, indicate the satellite twice passed near the polar cap in the 0000 to 0300 MLT sector at a latitude of 67° invariant latitude (IL) [*Sharber et al.*, this issue]. Meanwhile the equatorward edge of the oval remained near 55° for almost 20 hours on November 4. Return to more typical latitudes was a long, discontinuous process, punctuated by rapid equatorward excursions from November 4 to 8.

Official auroral electrojet (*AE*) calculations have not yet been completed for 1993 so we have produced pseudo estimates of *AU*, *AL*, and *AE* indices from the 78 available high-latitude ground magnetometer stations between 55° and 76° MLAT (Figure 2e, upper and lower curves, and Figure 2f, solid, respectively). An estimate of *AE* using the 12 official stations is shown by the dotted curve Figure 2f. By comparison the *AE* estimated from the official stations is smaller than that produced from the full complement of stations. Consistent with the argument that *AE* observatories do not sample electrojet perturbations at the peak latitude during large storms [*Feldstein*, 1992; *Cooper et al.*, 1995], this effect is most pronounced on November 4 when the auroral zone was expanded well equatorward of its normal location.

In the $AE_{(est78)}$ profile, we again see the stark contrast between the prestorm quiet and the extremely disturbed interval on November 4. Of some interest is the very small rise in $AE_{(est78)}$ just prior to 0800 UT, November 3. It follows by ~100 min the time that IMP 8 began sensing plasma of sufficient density to make interplanetary velocity and density measurements (Figures 4a and 4b). It also corresponds to the timing of the initial positive *Dst* values (See Figure 2g). Thus while the geomagnetic conditions remained quiet until ~1800 UT, November 3, there was an indication of changing interplanetary conditions as early as 0700 UT, November 3. Further changes are evident in the isolated disturbances at 1800 UT and 2300 UT, November 3. The former is associated with the final stage of the sector boundary crossing; the latter with the first substorm of the main phase and the likely passage of a solar wind transient (see discussion in next section). Shortly after onset the storm exceeded severe limits. The precipitous drop in $AE_{(est78)}$ (rise in $AL_{(est78)}$) just after 0100 UT, November 4, corresponds to about 1 hour of northward IMF. Subsequent to 0300 UT, November 4, $AE_{(est78)}$ rose to unusually high values indicting extreme disturbances in the auroral zone. Despite short intervals of northward IMF on November 4, which intermittently reduced $AE_{(est78)}$ below 1000 nT, the disturbance level remained extremely high and substorming was, for all intents and purposes, continuous. With some diurnal modulation, the magnetosphere and ionosphere experienced a classic high intensity, long duration, continuous, *AE* activity (HILDCAA) event [*Gonzalez and Tsurutani*, 1987] through November 8. Subsequently, the substorm frequency and intensity abated as the amplitude of the IMF fluctuations declined, and the solar wind speed slowed. On November 10, IMF fluctuations were sufficiently well separated so that individual substorms could be clearly tracked during the scheduled Radar World Day.

The *Dst* index provides additional insight into the storm progress. Figure 2g (solid) displays the *Dst* estimates from 27 stations and a pressure-corrected [*Burton et al.*, 1975] official *Dst* profile (dashed). The *Dst* positive (initial) phase began at 0800 UT, November 3. The very steep rise in *Dst* at 1200 UT, November 3, suggests a dipolarization of the magnetosphere (note increasing parallel field component sensed by GOES 7 in Figure 5a). At 1756 UT several ground stations reported a sudden impulse (SI) and sudden commencement (SC) (Solar Geophysical Data Prompt Reports, no. 593, part 1, 1994), however only minor geomagnetic activity commenced, the storm onset was several hours later. Thereafter *Dst* began a rather steep decline that arrested at ~2000 UT shortly after the IMF turned northward. The main phase *Dst* drop began at 2200 UT, as the IMF again turned southward, passing to negative *Dst* values at 2300 UT and reaching a local minimum just before 0100 UT on November 4. The most negative value of *Dst* (-116 nT) was achieved approximately 10 hours later when the combination of prolonged, strong southward IMF and very high speed solar wind flow and high solar wind density produced strong ring current effects [*Kozyra et al.*, this issue]. This value attests to the severity of the storm in that *Dst* is below −100 nT only 1% of the time [*Gonzalez et al.*, 1994]. The excursion to major (intense) storm status was brief (~ 5 hours) and occurred with the second peak of the main phase, consistent with the recent findings of *Yokoyama and Kamide* [1997]. Recovery phase commenced at 1200 UT, November 4 after passage of a second solar wind structure and extended over a 7-day interval to 0000 UT, November 12.

3.2 The Interplanetary Regime

Figure 3 presents the full storm view of the solar wind variations. Figure 4 provides more detail of the storm initial and main phases, with the IMP 8 and Geotail data sets superimposed for the 30-hour interval beginning 0600 UT, November 3. A parallel component magnetometer trace from GOES 7 and an energetic particle trace from the Geostationary Meteorological Satellite 4 (GMS 4) are also included to help with timing and interpretation. Because a continuous record of direct, unperturbed solar wind observations is unavailable for much of this interval, we use available magnetosheath Geotail observations as proxy data. With appropriate caveats (noted below) the magnetosheath data appear to be representative of the solar wind and the two data sets present the same large-scale view of the storm. Limited solar wind observations from IMP 8 were available on November 8-10 and these are used as a validity check for the Geotail observations. By comparison the IMP 8 solar wind density was higher by a few particles/cm^3. This slightly affects the dynamic pressure calculation in Figure 3c. We also make guarded use of the less than 18 hours of IMP 8 magnetosheath data available for the storm initial and main phases on November 3 and 4 to help fill the gaps when Geotail was inside the magnetosphere. The data gaps arise because Geotail was so near the magnetopause boundary that tail flux enhancements typical of southward IMF excursions often expanded the magnetosphere beyond the spacecraft position [*Nakamura et al.*, 1997]. They note that on November 4 the tail expansion was significant, but the duskward ($+V_y$) com-

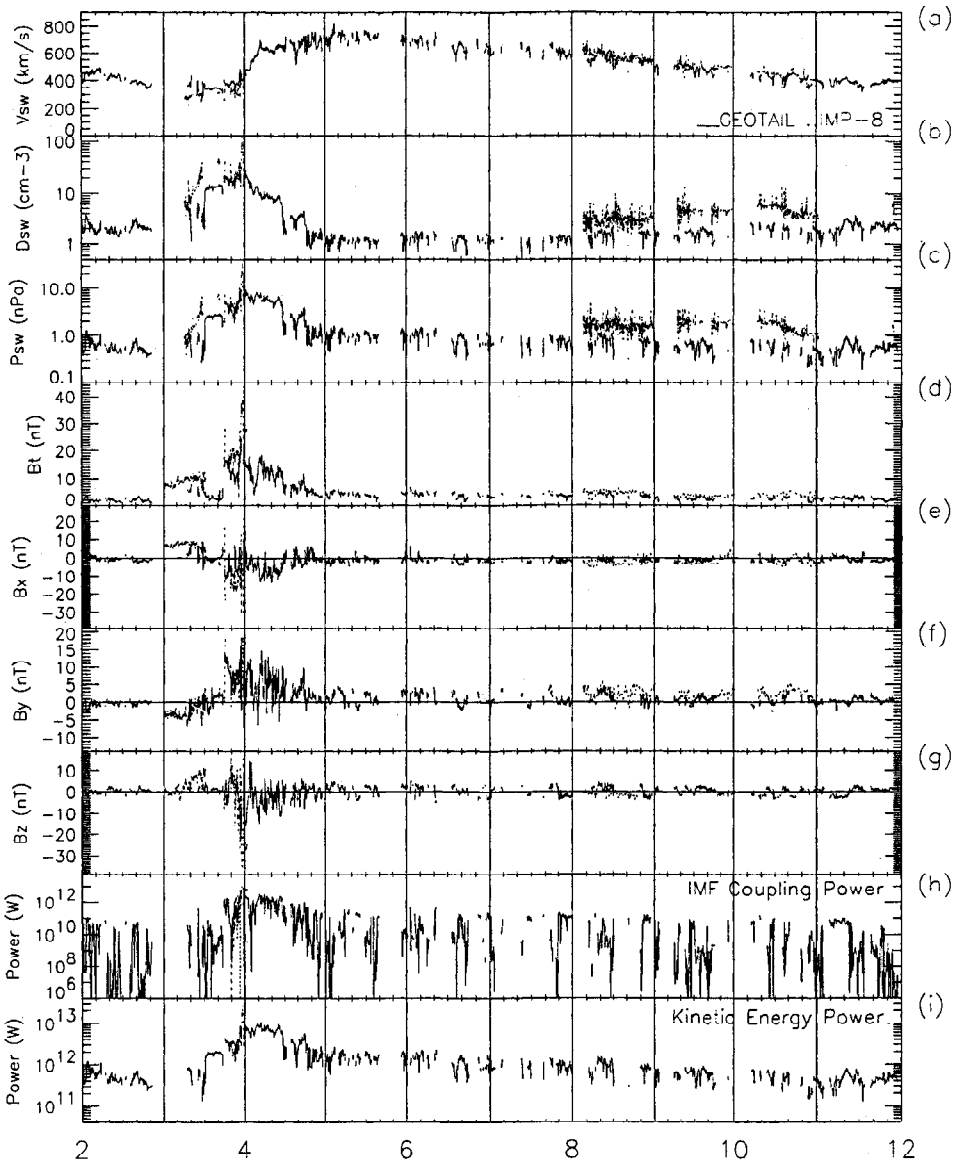

Figure 3. Observed and derived solar wind parameters: Geotail (solid) and IMP 8 (dashed). (a) The solar wind speed, (b) the solar wind density, (c) the derived dynamic pressure, (d) the total intensity of the magnetic field, (e) The B_x component), (f) the B_y component, (g) the B_z component, (h) The derived IMF coupling power, and (i) the derived kinetic power. All data are for November 2-11, 1993

ponent of the solar wind swayed the magnetotail away from the spacecraft. The indice data in Figure 2 lend credence to the idea that many of the data gaps in the Geotail record were associated with intervals of southward IMF.

3.2.1. Data reconciliation. At the beginning of the storm, IMP 8 and Geotail were located about -30 R_E and -207 R_E, respectively, tailward of the Earth (see Figure 4 of *McAllister et al.* [this issue]). Absence of Geotail data in our figures indicates the satellite was in the magnetotail. Because of the large spatial separations between the satellites themselves, and between Earth and the satellites, we have elected to reconcile the data from both satellites to "Earth passage time." The temporal reconciliation is roughly -10 min for IMP-8 and roughly -1 hour for Geotail, although these values vary due to the high solar wind speeds after storm onset.

The IMP 8 location behind the bow shock should lead to low-speed observations and high density and field observations relative to those from Geotail. Such was the case: Figure 4a shows that IMP 8 speed observations are ~20% smaller, and Figure 4d shows the total field intensity observations are ~40% larger than those of Geotail. The IMP 8 density observations (Figure 4b) are ~30% above those recorded by Geotail, and are reasonably consistent with recent model results from *Slinker et al.* [this issue]. On the basis of MHD model output, they find that IMP 8 magnetosheath B_z and B_t values are 30%-40% larger than those of the unperturbed solar wind. Limited comparative data available for IMP 8 and Geotail from 0000 to 0100 UT on November 4 (see Figures 4d and 4g) indicate this enhancement factor is reasonable. The minimum southward field value of -36 nT

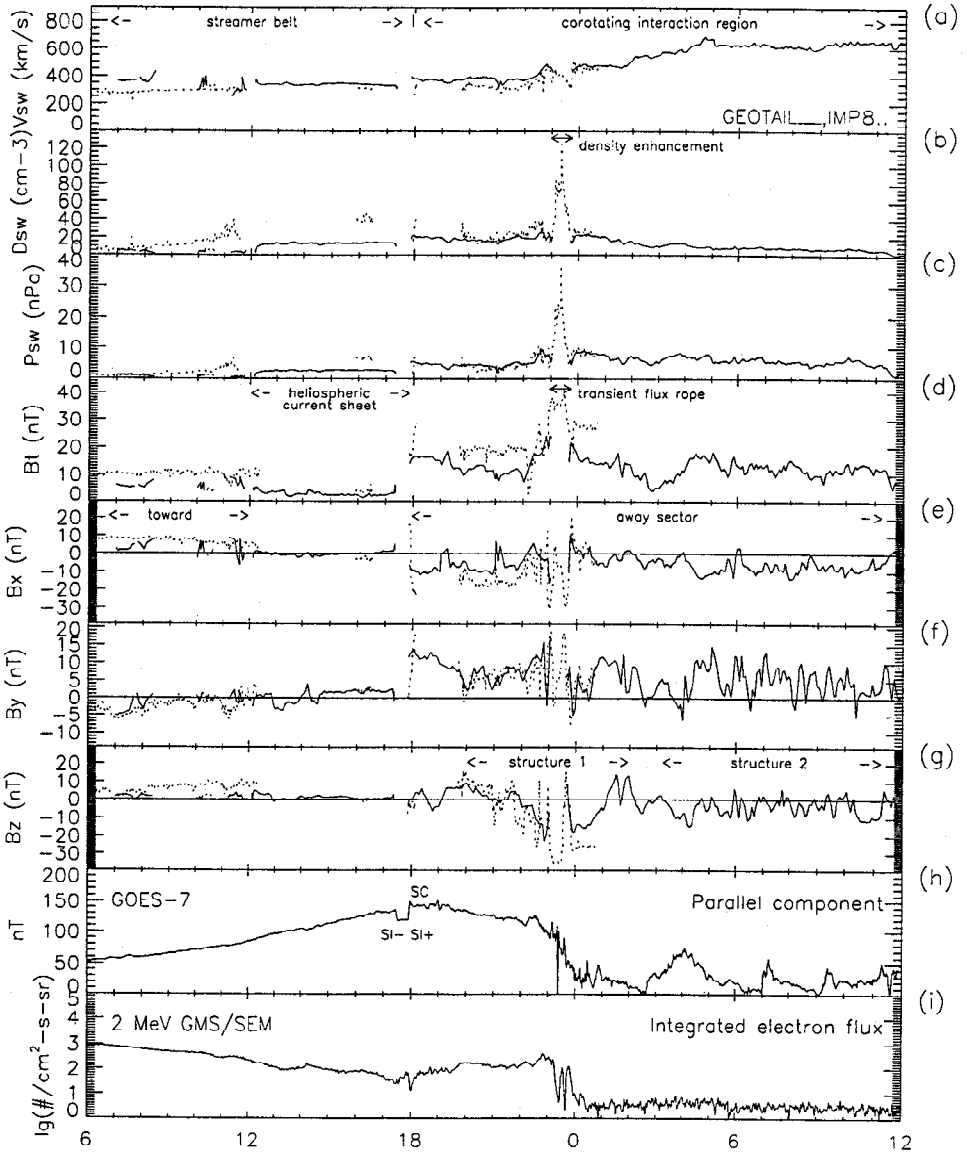

Figure 4. Observed and derived solar wind parameters: Geotail (solid) and IMP 8 (dashed). (a) The solar wind speed, (b) the solar wind density, (c) the derived dynamic pressure, (d) the total intensity of the magnetic field, (e) the B_x component), f) the B_y component (g) the B_z component, (h) the parallel magnetic field component observed by GOES 7, and (i) integrated flux of ≥ 2MeV electrons observed by GMS. All data are for 0600 UT November 3 to 1200 UT November 4, 1993.

observed by IMP 8 between 2320 and 2340 UT likely translates to a more realistic IMF B_z value of ~-25 nT, and the total field intensity for that interval is likely to be closer to 30 than 40 nT.

3.2.2. Solar wind structures. Solar wind speed (Figure 3a) was near normal on November 2, but early on November 3, Geotail data show speeds dropping as low as 350 km/s coincident with rising density values characteristic of the streamer belt [*Gosling et al.*, 1981]. This slow dense flow yielded, in a series of discontinuities, to very high speed flow on November 4. By early on November 5, the speeds momentarily reached 800 km/s. Figure 3a shows that return to normal flow speed required almost 7 days.

The density and dynamic pressure and IMF profiles (Figures 3b-3g) were complex but decipherable in terms of a CIR. An IMF "toward" sector ($B_x > 0$, $B_y < 0$) was clearly present prior to 1200 UT, November 3. Between 1200 and 1800 UT, November 3, the IMF components were all nearly zero, producing a near void in the total field intensity (see also Figure 4). The field void and compensating rise in density, keeping total pressure constant, mark passage of a heliospheric current sheet (HCS) enveloping the sector boundary [*Winterhalter et al.*, 1994]. After the SC at ~1800 UT, a new regime with $B_x < 0$, $B_y > 0$, and B_z oscillating about zero, arrived. The new "away" sector was one highly favorable to geomagnetic activity. After 2000 UT, November 4, the low densities associated with the high-speed stream proper appeared. This low-density plasma regime prevailed through the remainder of the interval. The profiles in Figures 3d-3g show a strong, compressed field late on November 3 and during all of No-

vember 4, followed by highly Alfvenic fluctuations on November 5-7 and a more relaxed field state during November 8-11.

Figure 4 depicts the primary features of the solar wind during the early portion of the storm. After passage of the HCS the higher density, increased field strength, and changing field orientation indicated arrival of the CIR Within the CIR are two structures which *McAllister et al.* [this issue] associate with separate eruptive arcade events at the Sun, which are strong CME signatures. The first structure was in the moderate-speed flow with passage between 2000 UT, November 3 to 0200 UT, November 4. The other was in the faster flow with passage between 0300 to 1200 UT, November 4. Embedded within the first structure was a transient enhancement of density and field strength (2305 - 2355 UT, November 3) which gave rise to the intense storm onset. *McAllister et al.* [this issue] investigated the characteristics of this enhancement and found it to be consistent with a noncompressive density enhancement and magnetic flux rope. The second structure was more evident in the field and composition changes than in the density record. At its leading edge were substantial composition changes including the appearance of He^{++} and heavy, highly ionized solar wind primary ions [*Lui et al.*, this issue]. Thereafter for about 9 hours the composition was anomalous, the flow angle was strongly duskward, the density was high, and the IMF exhibited strong turbulence, while the solar wind speed rose. It was during this interval that a superdense plasma sheet modulated the ring current [*Borovsky et al.*, this issue; *Kozyra et al.*, this issue] and significant regional and global ionospheric perturbations occurred [*Bust et al.*, 1997, *Ho et al.*, this issue; *Sharber et al.*, this issue; *Richards and Wilkinson*, 1998].

Figures 3h and 3i show estimates of the power extracted by interaction of the IMF with the Earth field and by kinetic energy due to plasma flow past the Earth. The epsilon parameter ε of *Akasofu* [1981] gives rise to power due to IMF coupling

$$v\, B^2 \sin^4(\theta/2)\, c^2 4\pi\varepsilon_0 * \text{area}.$$

While power due to the flow yields:

$$(\rho v^3) * \text{area},$$

where θ is the IMF polar angle measured from the z axis, ρ is solar wind mass density, v is velocity, and area is $(7\ R_E)^2$.

There was more than an order of magnitude increase in IMF coupling power with the arrival of the new sector boundary and another order of magnitude increase with the arrival of the density transient. The peak IMF coupling power value of $\sim 10^{13}$ W with the transient passage may be slightly overestimated due to reliance on IMP 8 magnetosheath data, yet the value is not unreasonable compared to Akasofu's [1981] value for a storm of similar intensity. Values of 5×10^{12} W prevailed during the main phase of the storm, while recovery phase values were $\sim 10^{11}$ W. In agreement with the *Akasofu* [1981] examples, kinetic power generally exceeded IMF coupling by at least a half order of magnitude. The difference may in fact be larger since the Geotail density is probably low compared to the unperturbed solar wind by a few particles/cm^3. For our energy budget calculations (section 6), we multiply the Geotail density, and hence kinetic power, by three to account for lower Geotail magnetosheath estimates.

3.2.3. Prestorm and storm onset. Prior to 1730 UT, November 3, geomagnetic quiet prevailed. At ~1730 UT, ground and satellite magnetometers (see Figure 4h) recorded a negative sudden impulse (SI-). A small but significant energetic particle perturbation registered at the dawnside location of GMS 4 just after the SI- (Figure 4i). Nearly simultaneously the Kyoto HF Doppler radar observed a frequency decrease, which T. Ichinose et al. (unpublished manuscript, 1998) associate with negative-impulse magnetospheric field decrease and subsequent upward motion of ionospheric electrons. Twenty-five minutes later the trailing positive SI (SI+) occurred (see Figure 4h). A sharp HF frequency increase accompanied the positive impulse. The long interval of geomagnetic calm ended with a series of small substorms. Just after 1900 UT, the IMF turned northward and another 3-hour period of geomagnetic calm ensued. Prolonged enhanced geomagnetic activity began at 2200 UT when the IMF turned strongly southward. Convection maps derived from SuperDARN coherent backscatter radars showed an unusually strong dusk-convection vortex developing within the first few minutes of the southward IMF interval (K. Baker, personal communication, 1996). Numerous ground- and space-based observatories noted an increase in geomagnetic activity and ionospheric convection. Geomagnetic activity was still increasing when the edge of the density transient arrived at 2305 UT.

The extreme values of density and field in the noncompressive density enhancement, observed by IMP 8 between 2305 and 2355 UT on November 3, are of primary concern to this study because they play a significant role in explaining the global disturbance. During that time, the total field intensity was high and the IMF components (Figures 4c-4g) showed rotations consistent with a compact flux rope [*Chen et al.*, 1997]. Between 2315 and 2330 UT, the average density value was ~80 particles/cm^3 and the maximum value was 125 particles/cm^3. Since Geotail abruptly entered the magnetotail at storm onset due to impulsive tail flapping, no corroborating magnetosheath data are available during passage of the transient. Although Geotail did not directly sample the field and plasma of the transient, immediately after the transient passed, Geotail reemerged into the magnetosheath and sampled significantly heated solar wind particles (M. Nakamura, personal communication, 1996).

At 2307 UT, the magnetopause passed over a LANL geosynchronous satellite located near magnetic noon. Rough calculations show that an unperturbed solar wind density value of ~100 AMU/cm^3 is required to balance the magnetopause at that location. More sophisticated modeling indicates that the large IMP-8 density values are reasonable and should result in a magnetopause crossing for a satellite located near noon MLT [*Slinker et al.*, this issue; J. Freeman, personal communication, 1997]. The LANL satellite stayed in the solar wind for more than half hour, while the transient passed, and measured compressed magnetosheath densities of ~ 190 particles/cm^3 at 2321 UT [*Borovsky et al.*, this issue]. The downward spikes in Figures 4h and 4i at 2322 UT indicate the GMS satellite, located at ~0900 MLT, and the GOES satellite, located at ~1630 MLT, also encountered the magnetopause at 2322 UT (H. Singer, personal communication, 1997). These geosynchronous satellites saw brief multiple crossings for 2 min (GOES 7) and for 20 min (GMS 4). The LANL satellite reentered the boundary layer from 0006 to 0027 UT on November 4. This event occurred after the den-

sity enhancement had passed and according to *Borovsky et al.* [this issue] was associated with a combination of dayside compression and flux erosion. After magnetosphere reentry, GOES 7 no longer observed 2 MeV particles at its near-dusk location. By 0030 UT, November 4, the GMS 4 satellite also observed the 2 MeV electron drop out. Magnetospheric modeling for this event suggests that magnetopause compression and or erosion to GEO may have significantly altered inner magnetospheric particle populations at storm onset [*Kozyra et al.*, this issue; *Freeman et al.*, this issue].

4. Storm Impacts and Geophysical Insights

4.1. Observations During Storm Onset

While the geosynchronous spacecraft were visiting the solar wind, dramatic effects were felt closer to earth. *Foster et al.* [this issue] report outer radiation zone energetic particle depletions beginning at 2315 UT and a sharp, narrowly confined eastward electric field enhancement at Millstone Hill (54° MLAT) at 2319 UT followed by F region uplift of 80 km at 2330 UT. On the basis of very low frequency (VLF) signal perturbations in a narrow auroral-latitude zone, they have timed the onset of energetic particle precipitation into the ionosphere at L=3.7 to 2332 UT. *Nakamura et al.* [1995] found evidence in SAMPEX data of enhanced energetic particle precipitation at the edge of the outer radiation belt just after storm onset. The Akebono satellite observed a nearly instantaneous central plasma sheet electron-temperature rise from 1.0 to 2.5 keV consistent with a strong adiabatic compression. *Richards and Wilkinson* [1998] suggest that prompt electric field effects were responsible for $F2$ layer uplift in the Australian sector at 0000 UT on November 4. GPS data show a northern hemisphere sudden TEC increase at the same time [*Ho et al.*, this issue]. *Foster et al.* [this issue] report DMSP measurements of vertical velocity of > 2500 m/s shortly after 0000 UT, satellite signatures of a narrow polarization jet or subauroral ion drifts (SAID) at 0030 UT, and enhanced precipitation of inner radiation belt electrons by 0200 UT, November 4. At 0252 UT UARS, at 55° IL and 2.8 MLT, encountered particle populations consistent with a stable auroral red (SAR) arc [*Sharber et al.*, this issue], a feature likely to accompany SAID events [*Foster et al.*, 1994b] and strong magnetopause compressions [*Shiokawa et al.*, 1997]. These observations along with those mentioned in section 3 point to a considerable disruption of the magnetosphere-ionosphere system with storm onset.

4.2. Preonset and Postonset Observations

4.2.1. Surface voltage fluctuations. Extreme geomagnetically induced voltage fluctuations like those observed during the March 1989 storm (~700 V) were not reported in any storm in 1993. Nonetheless, we deem it useful to establish a reference fluctuation profile for this storm. Figure 5a shows the voltage fluctuations on the midlatitude, undersea cable connecting Point Arena, California, and Hawaii. Geopotential variations are induced by ionospheric quiet day currents, tidal variations, and time rates of change in the magnetic field. Smooth diurnal variations associated with quiet-day overhead currents and ocean tidal features are evident on November 2 and 3. The sharp peak at 1800 UT, November 3 was a response to the SC. Irregular fluctuations during November 4-7 represent ground response to highly variable overhead storm currents. On the trans-Pacific cable (shown) the largest storm-driven fluctuations occurred in the main phase as the cable passed through the night sector (~1200 UT) on November 4. Geopotential fluctuations of roughly the same magnitude (10-15 V) occurred on the trans-Atlantic cable (not shown) between the United States and Europe, but the largest perturbations on that cable developed as it passed through the night sector during storm onset late on November 3. (Minor voltage fluctuations in transformers in the Finnish power system where reported at approximately the same time (A. Viljinen, personal communication, 1996). Rapid fluctuations began with storm onset and continued through November 8. On and after November 8, the variability diminished and quiet day currents and tides once again dominated the diurnal pattern. The geopotentials for this storm are in agreement with the overall induction relationship with the geomagnetic field and suggest that extreme overhead currents were not present at midlatitudes during this storm.

4.2.2. Ionospheric plasma signatures. Ionospheric aspects of the storm have been modeled by *Richards and Wilkinson* [1998] using the field line interhemispheric plasma (FLIP) model which calculates plasma densities and temperatures above 80 km along magnetic flux tubes connecting both hemispheres. The FLIP model reproduced well the dayside storm-induced increase in $F2$ density and the height of the peak $F2$ density. A combination of prompt electric field effects and aurorally generated wind surges were suggested as the causes of the increases. Model output and observations indicate that the height of the $F2$ layer, H_mF2, remained 50 km above quiet time values though November 7. They also found evidence of pronounced tidal effects which led to strong regional modulation of the height of the $F2$ layer within a few hours of storm onset. Tidal effects continued for several days. They offer anecdotal indication of a 200° K increase of midlatitude ionospheric daytime temperatures.

A recent run of the National Center for Atmospheric Research thermosphere-ionosphere electrodynamics general circulation model (TIEGCM) and data comparisons thereto, show global neutral temperature increases of ~200° K within 24 hours of storm onset, and an increase in the strength of equatorward winds during the storm peak [*Emery et al.*, 1997]. The model run also show a westward shift of global winds corresponding to the dynamo effect [*Blanc and Richmond*, 1980]. Although temperatures returned to prestorm levels after November 8, the TIEGCM run shows subauroral neutral wind disturbances continuing through the end of the storm period on November 11.

Beyond the prompt responses mentioned in section 4.1, there is evidence of aurorally generated wavelike oscillations with 200 km amplitude in $F2$ heights at several Australian stations [*Richards and Wilkinson*, 1998]. *Bust et al.* [1997] reported responses over the central United States beginning after 0200 UT, November 4. They chronicle the development of a very disturbed ionosphere during the passage of the second solar wind structure (0400-1200 UT). Patchy irregularities produced intense spread F signals (spread greater than 2 MHz) near 47° MLAT during the passage of the mid-America tomography chain under the nightside. They also report oscillations of the $F2$ layer, with the rise near 1200 UT exceeding 200 km in amplitude. Observations of the midlatitude trough of electron density were made near 50° MLAT with secondary depletions extending as far south as 35° MLAT. (Typical trough positions are close to 65° mag-

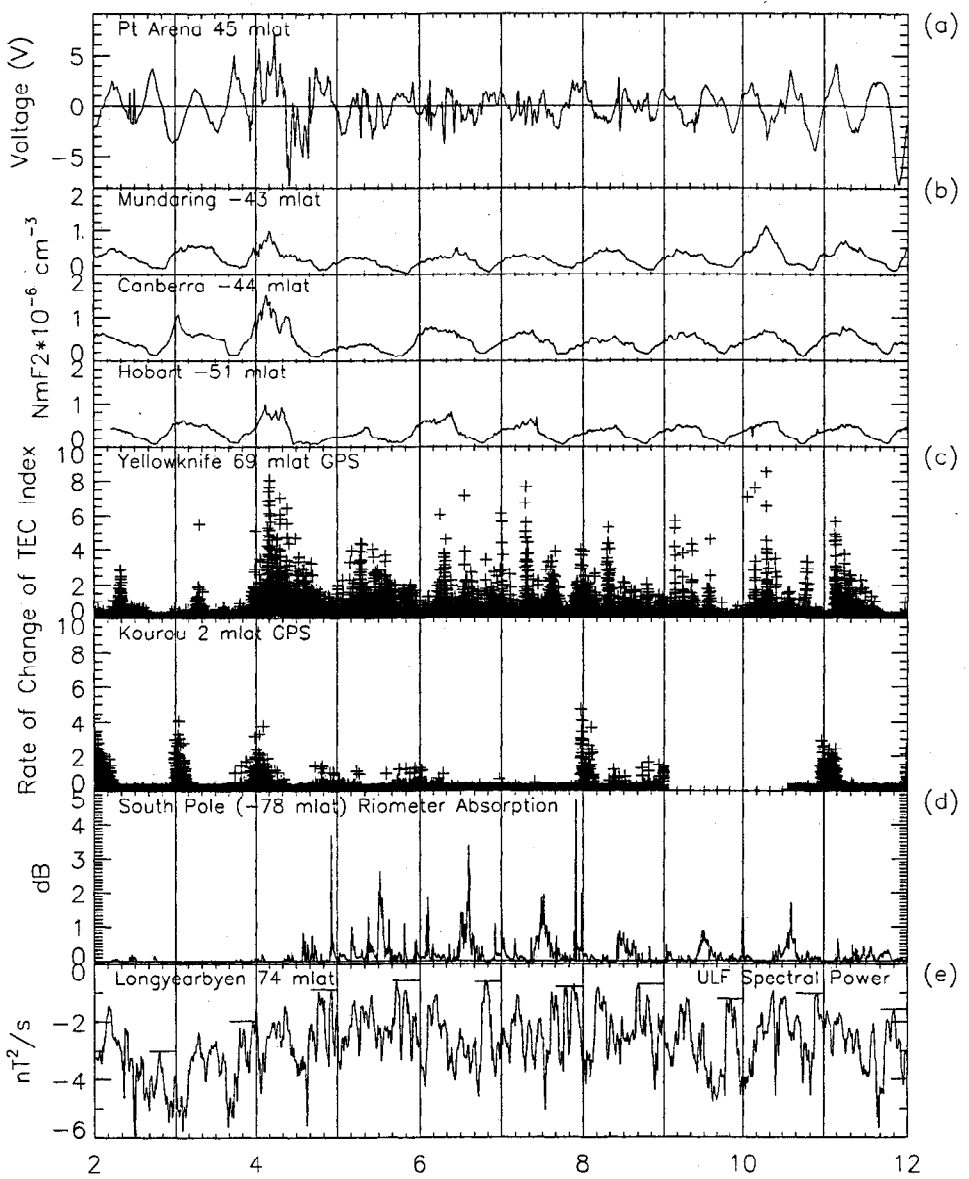

Figure 5. Ground-based observations: (a) voltage fluctuations observed on the transoceanic cable connecting Point Arena, California, and Hawaii, (b) peak density of the ionospheric *F*2 layer at Mundaring, Canberra, and Hobart, Australia, (c) The standard deviation rate of change of total electron content index (ROTI) for Yellowknife, Canada (auroral zone) and Kourou, French Guiana, (equatorial) South America. The index is a measure of GPS phase fluctuations, (d) The 20.5 MHz riometer absorption observed at South Pole Station, and (e) ULF spectral power observed at Longyearbyen, Norway. All data are for November 2-11, 1993.

netic). During the same interval, DMSP satellites recorded large changes in vertical drift velocities (more than 4 km/s over a 5° latitude path) also indicative of a highly disturbed topside ionosphere. Both *Richards and Wilkinson* [1998] and *Ho et al.* [this issue] report ionosonde data dropouts that compromised estimates of N_mF2.

Ho et al. [this issue] used the GPS space and ground network to sample TEC at a variety of locations around the globe. Their differential maps show clear storm progression effects during the 24 hours after storm onset. During the early hours of November 4, they found a 100% TEC increase in some northern hemisphere locations, indicating the development of a strong regional positive ionospheric storm phase. On and after November 5, a negative storm phase developed with some northern hemisphere locations experiencing an 60% decrease in TEC during the 60 hour event. *Richards and Wilkinson* [1998] report a similar, but more latitudinally limited, phenomena in the southern hemisphere. Figure 5b is a 3 panel illustration of the electron density variations measured by ionosondes at three Australian stations. The profiles show the expected diurnal variations associated with alternating sunlit and nighttime conditions. On November 4, an enhancement appears in the station profiles. Subsequently, on November 5, there was a suppression of peak electron density. These perturbations correspond to the positive and negative phases of the ionospheric storm. Minor storm effects were observed at these stations through November 7.

In addition to the TEC variation in the ionosphere, the GPS

satellites and their ground receiver arrays provided an interesting view of plasma irregularities during the storm. In Figure 5c, we present the rate of total electron content index (ROTI) observed by two GPS ground receiver stations: Yellowknife, Canada (auroral zone, 69° corrected geomagnetic latitude, CGLAT) and Kourou, French Guinea, South America (equatorial zone, 5°, CGLAT). This index is a measure of variability in the rate of total electron content change in the intervening atmosphere between the receiver stations and the satellite. Irregular structures of electron density distribution are responsible for signal fluctuations and sometimes receiver loss-of-lock on the satellite signal [*Pi et al.*, 1997]. The ROT Index for Yellowknife shows ionospheric irregularity variations only in the local midnight sector on November 2 and 3, consistent with a contracted auroral zone. With storm onset, plasma irregularities became ubiquitous and strong in the expanded auroral zone. Strong phase fluctuations developed between receivers and satellites on November 4 at Yellowknife and continued for a significant portion of the storm interval. At lower latitudes, Algonquin, Canada (57°, CGLAT) recorded strong phase fluctuations through 1200 UT on November 4. Minor fluctuations were recorded at 52° CGLAT by St Johns, Canada, indicating the equatorward extent of the auroral disturbance [*Aarons et al.*, 1997].

The equatorial data from Kourou illustrate different storm effects. At equatorial stations, plasma irregularities, thought to be driven by Rayleigh-Taylor instabilities [e.g., *Kelley*, 1989], give rise to TEC fluctuations at approximately dusk each day as a result of postsunset enhancement of upward E x B vertical drift [*Heelis et al.*, 1974; *Farley et al.*, 1986]. Such dusk effect fluctuations were present during the early UT hours on November 2 and 3. With storm onset the ROT Index indicated a longer interval of plasma irregularities. However, once into the recovery phase these irregularities diminished until November 8 when they returned to a more normal distribution. The diminution of irregularities during the recovery phase may indicate a suppression of the Rayleigh-Taylor instability. *Maruyama and Matuura* [1984] and *Mendillo et al.* [1992] report that storm time enhancements of equatorward meridional wind at low latitudes can play a role in reducing the instability growth rate. Thus strong geomagnetic storms may initially enhance and then subsequently dampen equatorial irregularities and their impacts on navigation.

For this event, the long-lasting irregularities at storm onset suggest a longitudinal expansion of the irregularities. At least two possibilities exist: development of extensive thin sheets of irregularites in the eastward drifting plasma, or the development of a system of towering plumes initiated by zonal electric field penetration during the early storm phase [*Aarons et al.*, 1997, Figure 1b]. *Aarons et al.* [1997] report that the irregularites covered at least 20° of longitude and argue, based on latitudinal extent of the scintillations, that a plume or plumes extended to an altitude of at least 1400 km.

4.2.3. Riometer observations. Figure 5d shows the 20.5-MHz riometer absorption observed at South Pole, Antarctica. South Pole station, (~-74 ° MLAT), is nominally in the polar cap during the nighttime hours (2130-0930 UT) and in the auroral oval or cusp during daytime hours. During magnetic storms, the polar cap boundary moves equatorward, thus effectively placing South Pole deeper into the polar cap on the nightside and possibly into the polar cap for some part of its passage through the dayside.

As expected, little absorption occurred on the quiet days of November 2 and 3, but interestingly, there were more than 12 hours with minimal absorption during the storm onset and peak on November 4. Significant absorption did not occur until after start of the storm recovery phase. During the storm main phase (~0000-1200 UT, November 4), South Pole was primarily on the nightside (~2130-0930 MLT). The absorption usually observed at South Pole, on the nightside results from the poleward expansion of substorm electron precipitation into the polar cap. Such precipitation can at times reach magnetic latitudes of 80° or higher [e.g., *Weatherwax et al.*, 1997]. Substorms were occurring during the first half of November 4 as judged by the high levels of *AE*. The absence of absorption at South Pole during that time, therefore, is attributed to geometrical considerations. That is, given the unusual expansion of the polar cap as revealed by the UARS, DMSP, and Akebono observations, the substorm poleward expansions did not reach latitudes as high as South Pole.

The absence of absorption at South Pole during the storm main phase on November 4 stands in marked contrast to that observed in response to the other magnetic storms in this recurrent sequence. South Pole was mostly on the nightside during the main phase intervals of those storms and recorded significant levels of absorption in most instances. It seems likely that equatorward expansion of the polar cap boundary was not as dramatic or as severe for these storms as it was for the November storm, permitting the poleward penetration of substorm precipitation to reach the latitude of South Pole station. Thus the lack of absorption at South Pole during the first half of November 4 stands out as an interesting effect of this storm, consistent with other information about the location of the polar cap boundary.

During storm recovery, broad absorption maxima occurred daily near 1200 UT as the station rotated into the dayside oval. Peak absorption events occurring early or late in the UT day were associated with substorms. Extreme, isolated absorption events occurred at ~2200 UT on November 4 and 7. The latter event late on November 7 was apparently due to a localized substorm effect, occurring shortly after a southward turning of the IMF and with a rise in low-energy particle precipitation (Figure 6e). The strong absorption was not observed at Iqluit, Canada, the conjugate riometer station in the northern hemisphere. The former event, however, was observed over large regions of the auroral zones and was coincident with the largest riometer absorption event of 1993 at Sondrestrom, Greenland [*Stauning*, this issue]. Prior to this unusual high-latitude disturbance, extreme convection distortion indicating a highly twisted magnetotail field was mapped with the assimilative mapping of ionospheric electrodynamics (AMIE) procedure. With substorm onset the convection distortion almost instantaneously relaxed. [*Stauning*, this issue]. Also associated with the event were observations of auroral light (630 and 558 nm) in the southern field of view of the meridian scanning photometer at Eureka, Canada, just above 84° IL (D. McEwen, personal communication, 1996). Stauning's modeling of this intense riometer absorption event suggests that repeated energization of thermal electrons can produce intense beams of 10-30 keV electrons. Interactions of these accelerated electrons with the upper atmosphere subsequently produced extreme and impulsive riometer absorption events during the substorm.

4.2.4. Waves. Ground-based observations showed systematic variations of ULF wave power with passage of each

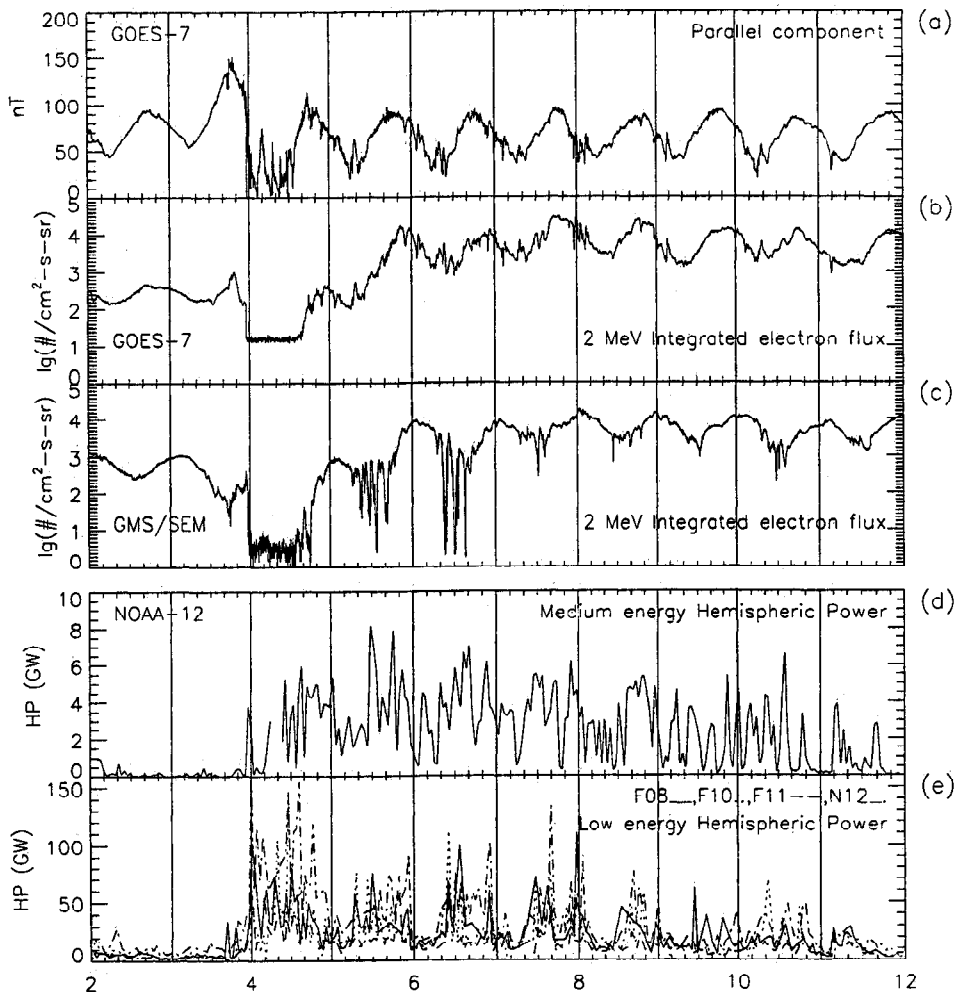

Figure 6. Satellite observations: (a) The parallel magnetic field component observed by GOES 7, (b) integrated flux of ≥ 2 MeV electrons observed by GOES 7, (c) integrated flux of ≥ 2MeV electrons observed by GMS 4, (d) the estimated hemispheric particle precipitation power derived from observations of NOAA 12 medium energy electrons, (e) The estimated hemispheric power derived from DMSP and NOAA 12 low energy electrons. All data are for November 2-11,1993.

high-speed stream in late 1993 [*Engebretson et al.*, this issue; *Rostoker*, 1995]. Figure 5e shows the 24-hour ULF record of spectral power observed in the 2-7 mHz band by the magnetometer at the near-cusp (~75° MLAT) station, Longyearbyen, Norway. The data show power rises when the station moved under the cusp (~0800 UT) and the nightside auroral zone (~2000 UT) and power decreases in other local time sectors. To better illustrate the overall trend in the data, we have drawn a bar over the peak value associated with transit through the nightside auroral zone. The Engebretson et al. study focused on dayside power increases. We show that nightside power was similarly affected. When the solar wind speed exceeded 650 km/s (Figure 3a), ULF spectral power peaks met or exceeded 0.1 nT^2/s. Peak spectral power dropped as solar wind speed approached 400 km/s on November 11.

The ULF data from the dayside transit on November 4 help us establish the case for an unusual polar cap configuration during at least part of the main phase. Between 0600 and 1000 UT, November 4, Longyearben passed near the dayside boundary as indicated by spectral features in the data [*McHarg et al.*, 1995]. This corresponds to the peak in integrated power seen at 0800 UT in Figure 5e. Near-simultaneous Akebono data (Figure 2d) indicate the dawn-dusk poleward boundary of the auroral zone was also near 75° MLAT. However, UARS data place the nightside poleward boundary near 66 ° MLAT. Thus, while the nightside auroral boundary was unusually distended, the dayside and dawn-dusk auroral boundaries were not. Simultaneous geosynchronous field observations show a significant dipolarization of the dayside field lines during this time.

4.2.5. Plasmasphere. Plasmaspheric behavior for this storm has been chronicled in several studies. Typically, the LANL geosynchronous satellites observe the plasmaspheric evening bulge once per UT day, however, during the pre-storm period the plasmasphere was inflated and observed at all local times at GEO [*Borovsky et al.*, this issue]. With storm onset, plasmaspheric material rapidly convected toward the dayside magnetosheath where plasma drainage was observed by the noontime LANL satellite which had exited the magnetosphere during passage of the density and field transient. The plasmasphere was apparently reduced in size for

most of November 4; there were no observations of plasmaspheric material by geosynchronous satellites on that day. Thereafter LANL satellites encountered the evening bulge, indicating a return to more normal conditions. Confirmation of the reduced plasmasphere is provided by *Hoogeveen and Jacobson* [1997], who observed nighttime geosynchronous satellite-to-ground signal fluctuations which they interpret as indicators of inner plasmaspheric ($2 < L < 2.5$) irregularities. These irregularities were apparent only in the storm recovery phase (in this case after 1200 UT, November 4) when the inner plasmasphere was likely to be relaxing back to its normal state. They show significant irregularities were present in the local midnight hours of November 5-7. Consistent with a reduced plasmasphere during the early recovery phase and a gradual expansion back to its prestorm size, they report irregularities closer to Earth in the early recovery phase and further away later in the storm.

The Freja satellite observed plasmaspheric ULF waves at 20 mHz to 4 Hz. *Mursula et al.* [1996] report intense ion-cyclotron waves near 67° MLAT during the compressional phase of the storm. With storm onset the active wave region moved to 50-55° MLAT and then slowly returned to high latitudes during recovery phase, also consistent with the expected movement of the plasmapause during the storm.

4.2.6. Geosynchronous field. The magnetometer onboard GOES 7 measured only the parallel component of the magnetic field during this interval. Figure 6a shows the variations associated with the dayside dipolar and the nightside stretched field, respectively. The satellite passed through local noon at ~1930 UT each day (LT=UT-0730). On November 3, the solar wind ram-pressure increase associated with the heliospheric current sheet and the leading edge of the CIR, produced additional dipolarization of the dayside field (note values in excess of 100 nT). A small, but notable, decrease in field strength accompanied the SI-/SI+ pair at 1730-1800 UT on November 3 (see Figure 4h for higher resolution). At 2232 UT, the satellite momentarily observed a southward field component as it exited the magnetosphere. Upon immediate reentry the satellite observed increasingly stretched field lines and continued to do so for the entire nightside transit (0000 -1200 UT, November 4). When the satellite returned to the dayside, it again observed enhanced dipolar field lines. Although the basic diurnal pattern recovered on November 5, small amplitude, high frequency fluctuations were superposed on the GOES daily variations between November 5 and 8, providing a subtle indication that the field remained disturbed. After 8 November the field returned to normal until a successive set of substorms on November 10 restretched the nightside field for a short time.

4.2.7. Magnetotail. The Geotail spacecraft made important measurements in the magnetotail as well as within the magnetosheath. *Kokubun et al.* [1996] report a tail lobe field value of 30 nT (more than three times the normal value) at -207 R_E on November 3 and 4 associated with strong tail compression due to enhanced solar wind parameters. *Nakamura et al.* [1997] used Geotail data to determine changes in the distant tail configuration and to estimate the radius and magnetic flux content of the tail. On November 2, the tail was unusually wide and the total pressure within the tail was low. With the arrival of the more dense solar wind plasma early on November 3, the magnetotail narrowed from 40 R_E in radius to ~25 R_E and remained so through the early main phase. The flux content rose sharply after the passage of the heliospheric current sheet and stayed high (> 1 x 10^{17} Mx) during the main phase. They attribute the combination of smaller tail radius and flux buildup to increased reconnection during the storm main phase. Consistent with many other observations of decreasing geomagnetic activity after 2000 UT, November 4, the tail flux decreased to prestorm values.

5. Particles: Trapped, Precipitating, and Disappearing

5.1. Medium- to High-Energy Particles

Energetic particle flux and density variations are of significant practical concern for this storm. *Foster et al.* [this issue] report that intense energetic electron precipitation into the atmosphere immediately after storm onset was responsible for nightside amplitude perturbations of VLF signals within a few minutes of storm onset. The precipitation effects continued for several hours and spread in longitude. Ionization effects have been modeled to depths near 30 km. Ionization there exceeded even that produced by strong galactic rays during solar maximum. Data from UARS Xray detector indicate more than an order of magnitude increase in integral bremsstrahlung Xray intensity in the northern hemisphere during the storm main phase. [*Sharber et al.*, this issue].

At GEO, the density of high energy electrons rose rapidly on November 4. Later while energetic electron fluxes where at their peak on November 7 and 8, penetrating background radiation compromised measurements by some instruments on LANL spacecraft [*Borovsky et al.*, this issue]. On 7 November a geosynchronous satellite experienced a satellite anomaly (55th Space Weather Squadron personnel, personal communication, 1996) most likely associated with the excessive energetic electron fluxes.

To illustrate the overall behavior of energetic electrons at GEO we show GOES 7 and GMS 4 integral flux profiles of > 2 MeV electrons in Figures 6b and 6c. Flux values were slightly low for most of November 2 and 3. After the SC, particle fluxes peaked for the day. Between 2325 UT, November 3 and 0030 UT, November 4, flux values dropped precipitously at GEO. The nearly flat lines in both curves on November 4 illustrate particle fluxes at or below the detectable level on each satellite. Consistent with the explanation of *Freeman et al.* [this issue], the satellite in the early morning sector, GMS 4, observed the earliest return of the 2 MeV population. Over the subsequent days, flux levels returned to and then exceeded normal levels by more than an order of magnitude. The > 2 MeV electron fluxes peaked on November 8 and remained high through midday on November 12. In addition to the large-scale storm variations, Figures 6b and 6c also show substorm variations. The high frequency, but small amplitude, fluctuations in the GOES 7 profile on November 4-7 and the reductions in the GMS 4 profile on November 5-7 are indicative of substorm scale perturbations. *Li et al.* [1997], *Borovsky et al.* [this issue], and *Freeman et al.* [this issue] show related flux profiles from the magnetospheric plasma analyzer (MPA) on the LANL spacecraft. Freeman et al. make a strong case for substorm control of the flux buildup.

Li et al. [1997] performed a multi-satellite survey of the energetic particle environment for this storm using observations from SAMPEX, GPS, and LANL spacecraft. Combined, these data sets showed a nearly total depletion of

> 3 MeV electrons at $4.0 < L < 8$ for more than 12 hours after storm onset. Further, they found that the reappearing particles returned to lower L shell values, with the less energetic particles returning first. The fluxes of the returning particles recovered to and exceeded prestorm levels at GEO by more than an order of magnitude. *Nakamura et al.* [this issue] completed a follow-up study on the SAMPEX 1 MeV electrons. At storm onset, they found significant L shell dependencies, with severe flux reductions at $4 < L < 7$. However, nearly simultaneously lower L shells experienced lesser reductions and even increases in flux. They infer that as a result of an unknown process, some energetic electrons are suddenly transported inward and scattered so that the pitch angle distribution is more field aligned.

Where do the electrons go at storm onset? *Li et al.* [1997] attribute inner zone particle losses to an adiabatic *Dst* effect which produces a redistribution in L, and outer zone losses to atmospheric precipitation and rapid magnetospheric boundary motions that allow magnetospheric particles to exit into the magnetosheath. *Korth and Friedel* [1997] reach a similar conclusion. *Kim and Chan* [1997] have simulated this behavior. For a magnetosphere compressed to within geosynchronous orbit, the opportunity for particle departure grows.

What replenishes the fluxes? *Nakamura et al.* [this issue] find evidence of a main-phase creation of an energetic electron population at the inner edge of the outer radiation belt which may serve to "seed" the subsequent enhancement of energetic electron flux at and around GEO. In the midrecovery phase of the storm, they report electron bursts associated with flux recovery of the 1 MeV electrons. *Borovsky et al.* [this issue] argue for a similar "source" populations created early in the storm process. *Freeman et al.* [this issue] offer an alternative explanation. They posit that the energetic electrons originate as the high energy tail of electrons injected by substorms and that ring current relaxation explains the slow, but steady, growth of high energy electrons fluxes during the storm recovery phase. They performed an in depth study of the spectral properties of low- and high-energy electrons for this interval and find recovery phase enhancements to be characterized by an increase of the power law spectrum of 100 eV to 1.5 MeV particles. *Sharber et al.* [this issue] also find a power law characterization of precipitating energetic particles.

Why are there a long-term rhythmic variations in the GEO fluxes? *Li et al.* [1997] found repetitive enhancements of energetic electrons in late 1993, which the solar wind and solar wind proxy data of this paper show were indeed associated with high-speed streams. We find there were energetic electron activations (for the >2 MeV level) for every onset of the primary and secondary high-speed streams (Figure 1i). We note that the primary stream, which had an "away" IMF orientation, always activated ≥ 2 MeV and ≥ 6 MeV electrons, although the December (winter) ≥ 6 MeV activation was weak. The secondary stream also activated ≥ 2 MeV electrons but was most effective in doing so when the IMF polarity was away or the speed was very high. The secondary stream activated the ≥ 6 MeV, only, when the IMF polarity was away. It would appear that activations of the highest energy electrons require not only high speed but also prolonged IMF conditions favorable to enhanced coupling between the solar wind and the magnetosphere. Such coupling may come in the form of direct antiparallel merging or perhaps via a magnetosheath process recently described by *Siscoe* [1997] which is reported to be effective during intervals of positive IMF B_y.

Why are there aperiodic enhancements of energetic electrons at low L shells? Injections into the "slot" region come from enhanced outer zone fluxes [*Russell and Thorne*, 1970], but *Korth and Freidel* [1997] remark that only the most intense geomagnetic storms affect the stability of the inner magnetosphere. The data in Figures 1a, 1g and 1h strongly suggest that some high speed streams produce such interactions. Others, perhaps lacking geoeffective density and IMF structures at their leading edge, do not. We know from this study that the density and IMF structures at the leading edge of the November 1993 were favorable to an intense storm and we speculate the same to be true for the August and September storm recurrences.

5.2. Medium- and Low-Energy Particles

Borovsky et al. [this issue] discuss impacts of the compressional phase of the storm and report the appearance of superdense ion and electron plasma sheets and unusually high plasma β values after storm onset. These conditions gave rise to severe spacecraft charging on November 4. They conclude that the superdense ion and electron plasma sheets were associated with the high-density solar wind and further that the high plasma β is a natural consequence of the high plasma sheet particle pressure. They attribute the strong nightside field stretching to diamagnetism generated by high ion plasma sheet pressure.

Kozyra et al. [this issue] show, via numerical simulation with the ring current atmosphere interaction model (RAM), that the high solar wind density gave rise to a dense plasmasheet which in turn became a controlling factor in ring current formation. They note that the factor of three density enhancement in the plasma sheet corresponded to a factor of three enhancement in the simulated ring current. They also pose an interesting feedback loop that may limit the magnitude of the *Dst* depression when strong magnetopause compressions allow potential ring current particles to escape the magnetosphere. Thus, a concern naturally arises about storm strength comparisons using the *Dst* index of the early main phase: while the *Dst* index may adequately measure the ring current strength, the ring current may not reflect the full impact of the storm if significant numbers of ring current particles have been lost to precipitation or drift beyond the magnetopause. The November 1993 storm simulation was also used as a realistic environment to investigate the potential effects of ion cyclotron waves on low- and medium-energy protons [*Kozyra et al.*, 1997]. With reasonable wave amplitudes, the model produced enhanced proton precipitation in the noon to dusk sector, which over the course of an hour, eroded the ring current and allowed an ~ 8 nT recovery of *Dst*.

Freeman et al. [this issue] modeled the early inner magnetosphere storm response for the main phase, including ring current formation at GEO with the Rice University magnetospheric specification model. Model results show loss of dayside particles at the time of the convection increase, plasma sheet injection of low-energy particles with an accumulation of low-energy protons and electrons around midnight and the formation of a ring current with sharp spatial gradients that fully encircled the earth within 10 hours of storm onset. RAM shows a more asymmetric ring current

structure with the asymmetry persisting during the first 16 hours of the storm.

Systematic enhancements of the precipitating energetic particle populations, like those associated with high-speed streams, may generate repeated mesospheric and stratospheric chemistry variations with long-term effects [*Callis et al.*, 1996a,b; *Codrescu et al.*, 1997b; *Frahm et al.*, 1997]. *Callis et al.* [1996a] used SAMPEX data from several of the late 1993 and early 1994 storms (four of the primary series) and found evidence of significant increases in Nitric Oxide (NO) from 70 to 120 km associated with precipitation of electrons into the upper atmosphere. In a companion paper, *Callis et al.* [1996b] modeled the effects of downward transport of NO on stratospheric ozone. Their calculations suggest ~30% mesospheric ozone depletion as an indirect result of prolonged high-energy electron precipitation events occurring in 1994. A recent paper by *Codrescu et al.* [1997b] gives a similar result. The UARS Halogen Occultation Experiment (HALOE) clearly shows mesospheric NO enhancement during the November 1993 event. *Crowley et al.* [this issue] report an order of magnitude increase in the NO mass mixing ratio at high latitudes during the first few hours of the storm. Preliminary modeling suggests at least a corresponding 30% depletion in mesospheric ozone (G. Crowley, personal communication, 1997).

A new hemispheric power calculation created from many years of NOAA-TIROS observations is useful for identifying intervals when the atmosphere may be subject to chemical perturbations associated with medium- to high-energy particle precipitation. Methods for deriving hemispheric power deposited by medium-energy particles (0.3 MeV to 1.1 MeV) observed by the NOAA satellites have been devised [*Codrescu et al.*, 1997b]. Figure 6d shows the estimated hemispheric power profile for the medium-energy particles precipitating into the atmosphere poleward of 65° MLAT. The actual number of precipitating particles is small, so power levels are in the 1-10 GW range. Storm onset produced a brief period of medium particle precipitation. Thereafter, the precipitating power dropped back to prestorm values for nearly four hours. One the basis of results from *Freeman et al.* [this issue], this reduction appears to be associated with the overall loss of energetic particles from the magnetosphere due to shifting drift paths and compression. Figure 5d suggests the redevelopment of medium-energy particle population within 4 to 6 hours. Figure 1 of Freeman et al. shows that a robust population of medium energy particles developed at GEO during the same interval. Thereafter, medium energy hemispheric power rose to levels occasionally in excess of 6 GW. During all NOAA 12 passes in 1993 such values were observed only 2% of the time. During this storm, they were observed ~12% of the time.

Hemispheric power estimates are regularly made from lower-energy (tens of keV) particle detectors aboard NOAA [*Fuller-Rowell and Evans*, 1987] and DMSP satellites. These particles are monitored mostly for their contribution to formation of the ionized auroral zone. Figure 6e illustrates the combined hemispheric power calculated from individual high-latitude pass segments (> 50° MLAT) of four polar orbiting satellites. The power profile for the lower-energy particles is similar to the profiles for most of the ionospheric indices. DMSP, NOAA, and UARS satellites observed unusually high precipitation power on November 4, with average values in excess of 50 GW. Particle power remained elevated through November 5. After November 8, minor, well-separated enhancements in the power were observed, consistent with slower arrival of IMF fluctuations in the solar wind. As a point of reference, the profiles on November 8-11 are representative of slightly to moderately disturbed conditions in the high-latitude region; the observed values on November 4 are roughly 3 times moderate storm values [cf. *Lu et al.*, 1996].

6. Assimilated Data and Storm Energetics

6.1. AMIE Results

We have included precipitating particle, ionosonde, DMSP ion drift, coherent radar, and ground magnetometer perturbation data sets in an assimilative mapping of ionospheric electrodynamics (AMIE) run [*Richmond and Kamide*, 1988; *Richmond*, 1992] and use these results to describe the high latitude response and partially determine the energy budget of the storm. AMIE patterns of electric field, horizontal and field-aligned currents, conductance and Joule heating have been mapped for each 10-min interval between November 2-11. Maps of current and convection patterns associated with storm onset have been presented by *Knipp and Emery* [1997]. *Ridley et al.* [this issue] and *Stauning* [this issue] present AMIE maps for other selected events within the storm. Figure 7 contains selected AMIE-derived results. To the best of our knowledge these profiles of cross polar voltage, effective conductance, field-aligned current, Joule and particle heating, are the first to cover a prolonged geomagnetic storm associated with a high-speed stream. The profiles agree well with the storm characterization in Figure 2.

Figure 7a shows the cross polar cap voltages in each hemisphere derived from available ground magnetometer data, DMSP ion drift meter (IDM) data, coherent and incoherent scatter radar data and digisonde drift data. Prestorm cross polar voltages were ~30 kV. The effects of the SC at 1800 UT, November 3 and passage of the density transient can be distinguished from the subsequent events. Near-continuous high voltages (> 100 kV) on November 4 occurred with the second solar wind structure and the leading edge of the high-speed stream. During the recovery phase, there was a slow downshift in the activity spectrum, with sustained high voltages (~70 kV), and indications of continuous substorming on November 5-8, followed by more intermittent substorms and convection enhancements on November 9-11 when the cross polar voltage was ≤ 50 kV. The voltages for the main phase of this event were about 60% of those estimated for the November 1981 severe magnetic storm [*Cooper et al.*, 1995] but substantially higher than those derived from a moderately disturbed equinox day by *Lu et al.* [1996]. They found average voltages of ~50 kV when the solar wind speed was low (< 400 km/s) and B_z was predominantly southward (~ -5nT).
We compared AMIE voltages to DMSP estimates from *Hairston et al.* [this issue], to main phase estimates from the Wiemer model [*Wiemer*, 1995] and to estimates of storm-onset voltages derived from a three-dimensional MHD model [*Slinker et al.*, this issue]. Consistent with the results from *Lu et al.* [1996], AMIE seems to underestimate peak storm voltages by ~20% compared to DMSP. Voltage estimates from less disturbed intervals are less affected. The Weimer model produces 30% higher voltage estimates during passage of the density transient but otherwise is in good agreement with

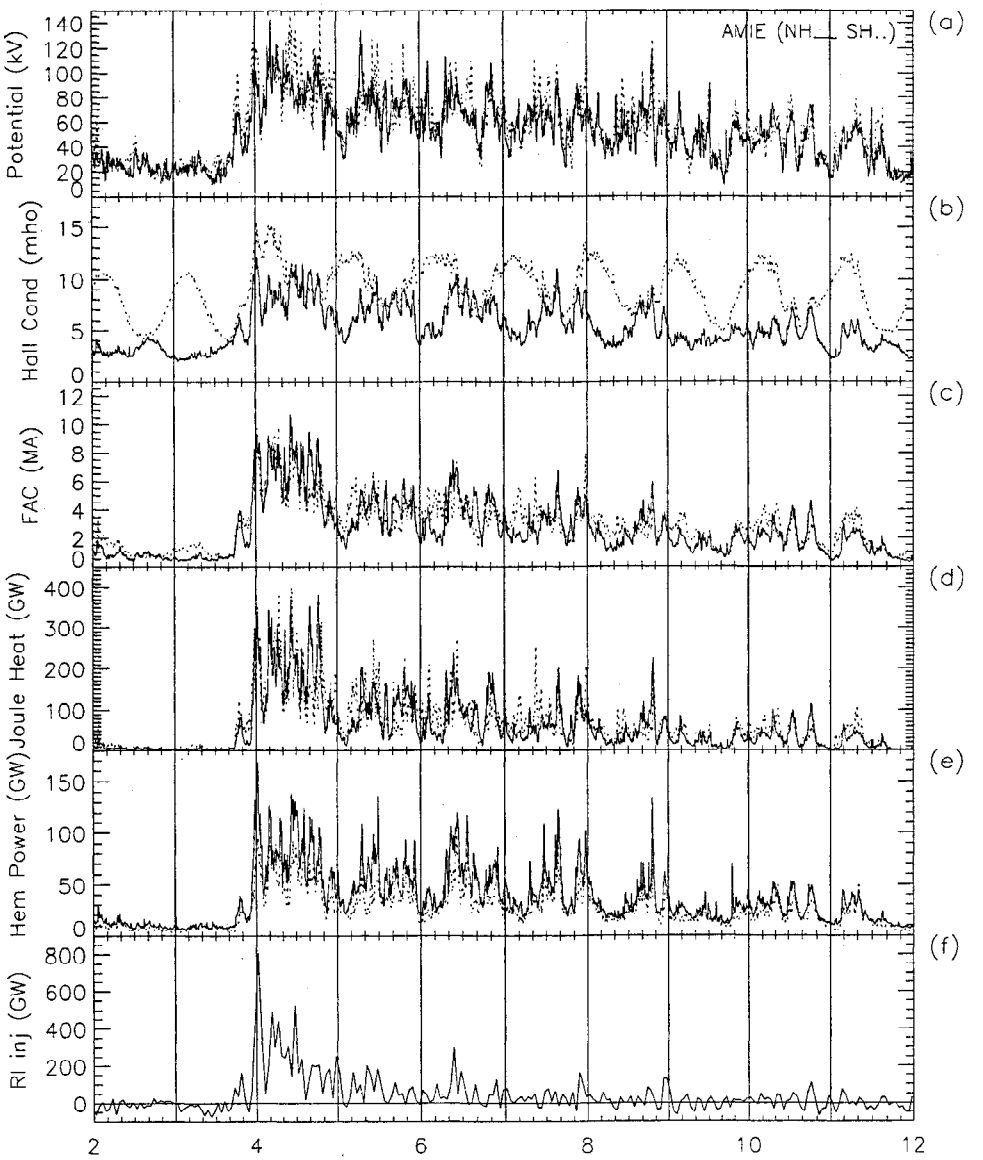

Figure 7. AMIE-derived ionospheric parameters for the northern (solid) and southern (dashed) hemisphere: (a) cross polar voltage, (b) integrated Hall conductivity above 55° magnetic latitude, (c) hemispherically integrated field-aligned current, (d) Joule heating, (e) Particle heating, and (f) ring current injection power. All data are for November 2-11, 1993.

AMIE results. The MHD model values are 100%-300% larger than the AMIE-derived values. The source of this discrepancy is not known at this time. See *Kozyra et al.* [this issue] for a comparison of voltage estimates.

Figure 7b shows the effective Hall conductance for each hemisphere. These values are the AMIE-derived, hemispherical average values (calculated above 50° MLAT) of height-integrated conductance. We note that the winter hemisphere experienced a wide range of conductance variations with the storm. Nightside precipitation effects dominated during much of the storm. On the quiet days, the effective Hall conductance in the northern hemisphere was about 3 mhos, on the most disturbed day it averaged ~7 mhos. Only during the main phase was the southern hemisphere conductance perturbed from the solar dominated diurnal pattern.

At each grid point in the AMIE domain, the divergence of the horizontal current is calculated to produce the local field-aligned current value. Figure 7c shows estimates of the hemispherically integrated downward field- aligned current, which by assumption is exactly balanced by upward currents. Quiet day values were ≤ 1 MA. For the most disturbed day, the average values exceeded 6 MA. More than 4 MA flowed during the active days, and approximately 2 MA flowed on the unsettled days. *Lu et al.* [1996] estimated average field aligned current flow on a moderately disturbed day to be ~3.5 MA. During the early portion of the UT day, there are interhemispheric differences in the integrated field-aligned currents. We attribute the differences to dipole tilting which enhances the conductance in one hemisphere relative to the other. *Hairston et al.* [this issue] find evidence of interhemispheric voltage differences lasting for several hours and argue that substantial field-aligned currents would be needed to support such differences on the closed field lines threading the polar cap. Their observations occurred in the early hours of No-

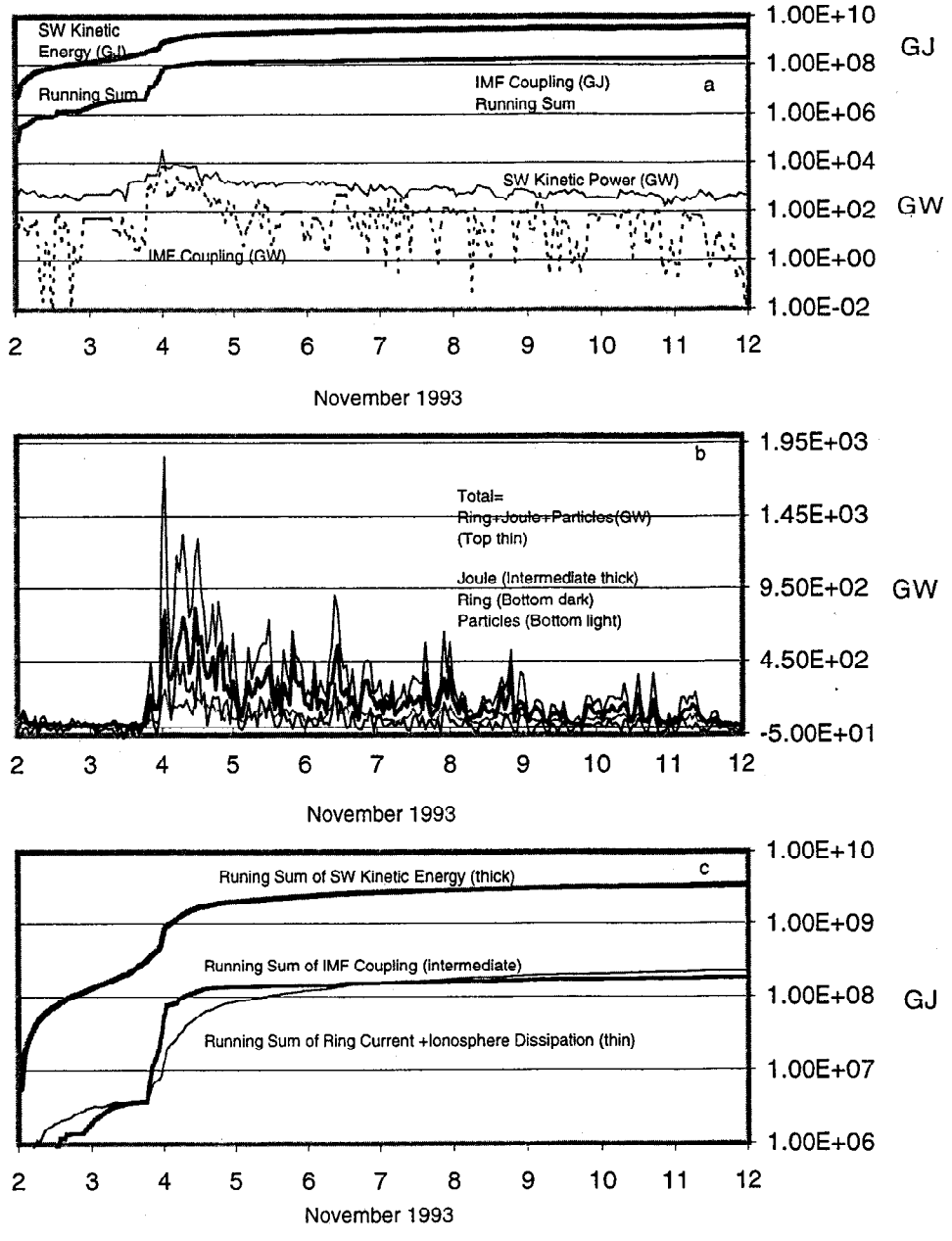

Figure 8. Storm energy budget. (a) Top curves: running total of kinetic energy and IMF coupling energy; bottom curves: hourly estimates of kinetic power and IMF coupling power, (b) hourly estimates of power dissipation by particle heating, Joule heating, and ring current injection, The top curve is the total power dissipated. (c) Running sum of solar wind kinetic energy input, IMF energy input, and ionospheric and magnetospheric energy dissipation.

vember 8 when AMIE results show ~25% difference in interhemispheric field-aligned current values.

Joule and particle heating (Figures 7d and 7e) give a clear delineation of the storm for the coupled magnetosphere-ionosphere. Joule heating was minimal prior to 1800 UT, November 3. A brief heating rise accompanied the SC and a very sharp 300 GW spike developed with the density transient. The sustained geomagnetic activity produced a daily heating average in excess of 200 GW on November 4, with numerous spikes near 300 GW, in good agreement with the Joule heating estimated by *Anderson et al.* [this issue] from UARS data. The Joule heating on November 4 is nearly 3 times the average value shown by *Lu et al.* [1996] for more modest events and about half that estimated by *Richmond et al.* [1998] for a large magnetic cloud event. While the solar wind speed remained above 600 km/s, the daily average values of Joule heating stayed near 100 GW. The globally integrated, AMIE-derived Joule heating for the storm period is ~137 PJ (60% of the total dissipation). Approximately 30% of this heating occurred on November 4. Joule heating contributed two and one half times the power of the precipitating particles to the auroral zone. Particle precipitation accounted for roughly 20% of the ionospheric energy budget on November 4 and 25% during the entire storm. Total ionospheric heating during the storm was ~ 190 PJ.

Richards and Wilkinson [1998] report a double-peaked rise

Table 1. Storm Energy Budget (PJ) for Intervals Ending at Times Indicated

Beginning Time 0000 UT Nov 2	0000 UT, Nov. 4	1200 UT, Nov. 4	0000 UT. Nov. 5	0000 UT, Nov. 8	0000 UT, Nov. 12
$U_{solar\ wind}$	640	1510	1830	2900	3260
ε	54.6	123.0	137.0	170.0	181.0
$U_{Particles}$	4.2	10.8	15.6	42.0	53.0
U_{Joule}	8.6	32.5	49.3	118.0	137.0
U_{ring}	0.4	15.2	21.8	37.0	38.0
$U_{total}=U_{part}+U_{Joule}+U_{ring}$	13.2	58.5	86.5	197.0	228.0
% U_{total} of $U_{SolarWind}$	0.02%	4%	4.5%	6.8%	6.9%
% U_{total} of ε	24%	48%	63%	116%	125%

of H_mF2 at some Australian ionosonde stations during 0000-0200 UT, November 4. They suggest electric field penetration drove the initial peak and an auroral zone neutral wind surge emanating from the impulsive Joule heating event at ~0000 UT on 4 November created the second. *Emery et al.* [1996] report that waves generated by impulsive heating can reach the equator within 2 hours. *Emery et al.*, [1997] find excellent agreement between observed and TIEGCM-modeled H_mF2 gravity waves. Five distinct surges driven by realistic AMIE-based Joule heating estimates are evident in the data and the model output for November 4.

Figure 7f shows 1 hour estimates of the ring current injection power estimated using the Dessler-Parker-Schopke ε formulation from *Akasofu* [1981]. The estimates are admittedly coarse due to the gaps in the IMF data and hourly averaging, so we get only a rough picture of the energy requirements for the ring current. By our estimates, ring current injection was the largest energy sink during storm onset. During the remainder of the main phase, ring current injection and ionospheric heating were of roughly equal magnitude. Thereafter Joule heating became the dominant energy sink for the storm. *Kozyra et al.* [this issue] provide a complete simulation analysis of the ring current development using RAM. They find the ring current injection energy based on the ε formulation to be nearly an order of magnitude too large for this main phase, but of the right magnitude for the overall storm input. Interestingly, they find the *Burton et al.* [1975] energy input formulation to be a better descriptor of storm main phase energy input, but it significantly underestimates energy input for the HILDCAA phase. This finding has important implications for storm budgets. Because our interest lies in providing the overall storm budget, we used the ε formulation for the ring current energy estimates.

6.2. Energy

Figure 8 and Table 1 present the energy budget for the storm. In Figure 8a we show the IMF coupling energy and power and kinetic energy and power data (from the formula in section 3.2.2 using hourly averaging and some minor interpolations) as well as the running sum of these values. Figure 8b shows the relative and total values of the storm power sinks. In Figure 8c, we show the running cumulative energy inputs and sinks, and in Table 1 we provide energy totals at various points in the storm. We have accounted for ring current injection, auroral electron precipitation and Joule heating as the major energy dissipation mechanisms. We have not accounted for the energy associated with precipitating ions which *Kozyra et al.* [this issue] show to be an order of magnitude smaller than that of precipitating electrons, nor the small amount of energy needed to drive atmospheric circulation, which *Lu et al.* [1995] estimate to be ~5% of available magnetospheric energy, nor the energy stored in the magnetotail or ejected with plasmoids. By our estimates, energy provided by magnetic merging during the storm main phase was roughly 4×10^{16} J greater than that dissipated (the difference is larger if indeed our ring current energy is overestimated. *Nakamura et al.* [1997] estimated that 5×10^{15} J (~10% of the difference) was stored in far-tail region during the main phase of the storm. Some of the remaining excess energy was likely associated with plasmoids and some may have been partitioned into the field configuration which was known to be anomalous in terms of orientation and stretching during the main phase. At the end of the main phase, we show the total energy dissipated to be ~60 PJ which is roughly 4% of the solar wind kinetic energy. The bulk of the energy dissipated, ~75%, went into the ionosphere. By the end of the storm the total energy dissipation was ~230 PJ with roughly 83% of that energy deposited in the Earth's ionosphere.

Figure 8c indicates that magnetic merging energy input was insufficient to cover the energy dissipated by the ionosphere and ring current after November 7. Because of the uncertainty and gaps in solar wind data, the possible over estimate of the ring current injection energy, uncertainties in the AMIE estimates of energy dissipation, and insufficient knowledge of the magnetotail energy storage and loss, we cannot make a definitive statement about the deficit or even be sure that a deficit truly existed. It appears likely that energy inputs and dissipation are fundamentally balanced, however if not, it is possible that required energy difference could be extracted from the solar wind kinetic energy during the HILDCAA phase of the storm. Further study of high-speed stream driven storms in the era of continuous solar wind coverage will be needed to determine if magnetic merging can, indeed provide all the required energy for a storm of this type and duration. *Lu et al.* [1998] are engaged in such an effort.

7. Summary

We and others associated with this extensive storm study have provided an origin-to-end view of this geomagnetic storm, tracing its effects from the recurrent coronal hole and nearby transient-generating regions, to geosynchronous orbit, to well within the Earth's stratosphere, and to cables on the

ocean bottom. We provide profiles of storm behavior that range from magnetic field and energetic electron perturbations at GEO, to profiles of high-latitude ionospheric parameters, to relatively new measures of plasma irregularities. We provide some evidence that immersion in a favorably oriented IMF sector may have impacts beyond the obvious enhancement of dayside reconnection. In Figure 1 we show that activations of energetic electron events appear to have an association with the appearance of a favored "away" IMF orientation in late 1993.

The early November 1993 was strong and had prolonged effects on the Earth's environment. This can be understood in the context of a 22-year solar coronal pattern and a 22-year cycle that allows prolonged access to high-speed flow and IMF field favorable to geomagnetic activity. (See Section 2 for discussion.) Strong, recurrent high-speed streams developed in the decline of solar cycle 22. We make a case for two streams in late 1993, one of which was particularly geoeffective as indicated by high magnetic indices and short-lived energetic electron flux enhancements at L=3 (See Figure 1). The November recurrence was accompanied by several key elements for geoeffectiveness: high solar wind density, rising solar wind speed, embedded solar wind transients with strong southward IMF, strong field compression ahead of the high-speed stream, and rapid IMF fluctuations with and after the stream arrival. We discussed the close links between the solar wind transients and the early main phase in sections 3 and 4. *Borovosky et al.* [this issue] and *Kozyra et al.* [this issue] argue that the high density strongly modulated and even controlled the inner magnetosphere and ring current dynamics.

Storm arrival was well anticipated but storm strength and prompt (early main phase) effects were largely unanticipated. Index values derived for the main phase of the storm put it in the top 25% of all geomagnetic storms. The extreme field and density fluctuations on November 3 were associated with a sub magnetic cloud-scale, noncompressive density enhancement [*McAllister et al.* this issue] with a flux-rope-like signature [*Chen et al.*, 1997]. A likely second transient structure passed between 0300 and 1200 UT on November 4, and was accompanied by enhanced levels of He^{++} and highly ionized heavy ions in the solar wind [*Lui et al.*, this issue], large total IMF intensity, and substantial field turbulence. On the basis of reduced size of the field oscillations after ~1900 UT, November 4, along with a significant reduction in density at that time and an expansion of the magnetotail radius [*Nakamura et al.*, 1997], it appears that the Earth emerged from the influence of the transients and came under the dominant influence of the high-speed stream.

Contributors to this study have shown that the storm set into motion an immediate chain of events that brought the entire dayside magnetopause to within geosynchronous orbit. Almost immediately, energetic electron (> 2 MeV) fluxes dropped below detectable levels at GEO [*Li et al.*, 1997] and the *Dst* index dropped precipitously. Magnetospheric electric fields penetrated to low latitudes and produced a near-instantaneous uplift of the nighttime F layer by 80 km [*Foster*, this issue]. In the same time frame, the magnetotail impulsively flapped and the magnetotail radius narrowed [*Nakamura et al.*, 1997], while the nightside field became extremely stretched [*Borovsky et al.*, this issue]. Equatorial plumes of plasma irregularities rose into the exosphere [*Aarons et al.*, 1997]. The equatorward edge of the auroral oval extended to 55° MLAT. Geopotentials on transoceanic cables and voltages in high-latitude transformers fluctuated. Extreme disturbances in the auroral and subauroral zones changed VLF propagation paths [*Foster et al.*, this issue] and produced 100% TEC perturbations in the northern hemisphere [*Ho et al.*, this issue]. Ionosonde data dropouts compromised or prevented estimates of N_mF2 at several locations [*Richards and Wilkinson, 1998*; *Ho et al.*, this issue].

Within 6 hours of storm onset, the poleward polar cap nightside boundary reached 66° IL and auroral zone heating produced equatorward propagating waves that generated rhythmic oscillations of the F layer height at midlatitude Australian ionosonde stations [*Richards and Wilkinson*, 1998]. Spread F disturbances were observed in the morning sector [*Bust et al.*, 1997]. Within 10 hours of storm onset, a positive phase ionospheric storm became evident [*Ho et al.*, this issue] and large vertical flow velocities were recorded by satellites at 800 km altitude [*Bust et al.*, 1997]. Auroral ground stations for GPS reported instances of strong signal fluctuation. Ionospheric trough perturbations were observed equatorward of 40° MLAT [*Bust et al.*, 1997]. Observations from low Earth orbiting satellites suggest more than 250 GW of Joule heating [*Anderson et al.*, this issue] and 50 GW of particle heating on November 4. The influence of deeply penetrating ionization was measured to depths of nearly 30 km [*Sharber et al.*, this issue]. As a result of energetic particle penetration into the mesosphere, nitric oxide levels rose markedly [*Crowley et al.*, this issue]. Within 12 hours of storm onset, geosynchronous spacecraft began to experience severe charging [*Borovsky et al.*, this issue]. During the first 12 hours of the storm energetic electrons were absent from geosynchronous orbit, but enhanced fluxes were observed near L=3 [*Li et al.*, 1997; *Nakamura et al.*, this issue]. Twenty hours after storm onset, the magnetotail radius widened indicating some magnetospheric relaxation [*Nakamura et al.*, 1997], but 3 hours later one of the most extreme substorm-related riometer absorption events of 1993 occurred at Sondrestrom, Greenland [*Stauning*, this issue].

Within a day of storm onset, modeled and inferred upper atmospheric temperatures above 300 km had risen by at least 200°K globally and the wind field was notably disturbed. More than 24 hours after storm onset a negative phase ionospheric storm developed with up to 60% TEC reductions [*Ho et al.*, this issue]. Over the course of the subsequent 3 days energetic electron fluxes at geosynchronous orbit rose by more than an order of magnitude above the prestorm values and more than three orders of magnitude above main phase values. A spacecraft anomaly was reported during the interval of high flux. For nearly the full recovery period of the storm, strong ULF wave activity was reported by ground- and space-based platforms [*Engebreston et al.*, this issue; *Mursula et al.*, 1996]. Traveling convection vortices and impulsive vortices were often observed by arrays of dayside magnetometers [*Zesta et al.*, 1995; *Stauning et al.*, 1995; *Ridley et al.*, this issue].

Our knowledge of the storm is not limited to observations. Physics-based and data assimilation-based models provided significant new insights regarding (1) the role of solar wind density as a storm control agent and the role of particle drift losses on *Dst* [*Kozyra et al.*, this issue], (2) the behavior of energetic electrons [*Freeman et al.*, this issue; *Li et al*, 1997], (3) global TEC behavior [*Ho et al.*, this issue], (4) penetrating energetic electron behavior and effects [*Sharber et al.*, this issue], (5) global ionospheric effects [*Richards and Wilkinson*,

1998], (6) substorm dynamics [*Stauning*, this issue], and (7) relative magnitudes of energy input and dissipation (this paper). The combined results from the first three studies listed above suggest that some "intense" storms may be initially under estimated by the *Dst* index if a significant fraction of potential ring current particles are lost to precipitation or drift beyond the magnetosphere due to a magnetopause compression.

This paper presented the first storm/HILDCAA profiles of cross polar cap voltage, Joule heating, integrated field-aligned currents and Hall conductance. The average Joule heating during the most intense phase of the storm was > 200 GW, approximately twice the average for moderate storms. We estimate that a total of ~137 PJ of energy was generated globally by Joule heating over the 10-day interval. More than 30% of this was generated within the first 24 hours of storm onset. Total energy dissipated was ~230 PJ. Integrated field aligned currents for the same day were 6 MA compared to 4 MA for the moderate storm days. Further, we developed a simple energy budget for the storm whose magnetic energy input is close to balance with the estimated Joule, particle and ring current sinks.

In summary, the November 2-11, 1993, magnetic storm event has provided the space physics community with the opportunity to merge a myriad of data sets for a comprehensive view of this magnetic storm specifically, and a broader understanding of magnetic storms in general. Although more work is possible and some questions are still unanswered, it is clear that recurrent high-speed streams, espeically those with embedded transients, can have enormous geo-effectiveness at Earth. We wish to thank all contributors for a successful storm study.

Acknowledgments. This research has been supported by NSF grant ATM 9613829. This work is the outgrowth of a coordinated effort amongst the national and international space weather community. Scientists from the CEDAR, GEM, and SHINE groups have participated in this event study. The CEDAR database is supported by the National Science Foundation. We have had many useful discussions with N. Crooker, H. Singer, A. D. Richmond, J. Kunches, G. Lu, K. Perymat, P. Stauning, and J. Aarons. We are especially grateful to J. Freeman of Rice University and D. Baker of the Laboratory for Atmospheric and Space Physics (LASP) for hosting workshops on this event and to C. T. Russell, T. Mesorrell, and G. Le of the University of California Los Angeles, for providing World Wide Web support and data archival. We are grateful to the following individuals and institutions for providing data to this storm study: World Data Center A for geomagnetic index and magnetometer data, World Data Center B for magnetometer data, World Data Centers C1 and C2 for geomagnetic index data, the Air Force Research Laboratory for the Auroral Boundary Index data, L. Frank (Geotail plasma data), R. Lepping (IMP 8 IMF Data), A. Lazarus, and K. Paularina (IMP 8 Plasma data). The IMP 8 data were provided by the MIT Space Plasma Physics Group and are publicly available by ftp or the WWW, M. Nakamura (Geotail B field and low energy particle data), T. Terasawa (Geotail data interpretation), M. Den at the Hiraiso Solar Terrestrial Research Center (GMS particle data), M. Hairston and R. Heelis (DMSP ion drift meter data and retarding potential analyzer data), K. Baker and M. Ruohoniemi (SuperDARN radar data and analysis), J. Scali and B. Reinisch (high-latitude digisonde velocity and electron density profiles), A. Green (International Real-Time Magnetic Observatory Network (INTERMAGNET) data), J. Dudeney, A. Rodger and M. Pinnock (British Antarctic Survey (BAS) magnetometer data and Halley Bay incoherent radar data), B. Fraser and G. Morris (Australian National Antarctic Research Expedition (ANARE)), C. Maclennan (Bell Laboratory midlatitude magnetometer data), E. Friis-Christensen, T. Morretto, P. Stauning, and B. Sitar (Danish Meteorological Institute Greenland Magnetometer Array data), J. Hughes (Magnetometer Array for Cusp and Cleft Studies (MACCS) magnetometer data), H. Luhr (International Monitor for Auroral Geomagnetic Effects (IMAGE) magnetometer data), L. Morris (National Geophysical Data Center Geomagnetic On-Line data), J. Olson (Remote Geophysical Observatory Network (RGON) magnetometer data), D. Orr and D. Milling (SubAuroral Magnetometer Network (SAMNET) magnetometer data), D. Detrick (South Pole Station magnetometer data), G. Rostoker and T. Hughes (Canadian Auroral Network for the Origin of Plasmas in the Earth's Neighborhood (OPEN) Program Unified Study, (CANOPUS) magnetometer data), S. I. Solovyev (Institute of Cosmophysical Research and Aeronomy magnetometer data), C. Szuberla (Lonyearbyen magnetometer data), O. Troshichev (Arctic and Antarctic Research Institute (AARI) magnetometer data), R. Clauer (monitor for auroral geomagnetic (MAGIC) effects magnetometer array data), A. Zaitzev (Institute of Terrestrial Magnetism Ionospheric and Radio Wave Propagation (IZMIRAN) magnetometer data), V. M. Mishin (Siberian Institute of Terrestrial Magnetism Ionospheric and Radio Wave Propagation (SIBIZMIR) magnetometer data), A. Viljanen (IMAGE magnetometer data and ground voltages), S. Vennerstrøm at the WDC C1 for Geomagnetism, Danish Meteorological Institute (PC index), T. Kamei (*Dst* index from World Data Center C2), W. Worthington (Boulder CO ground magnetometers and spectrograms), K. Shiokawa (210° Magnetometer Chain Data), R. Coles and D. Boteler (Canadian Bureau of Energy and Mines, Magnetic Observatory Network data), D. Chenette (UARS X-Ray data), D. Winningham (UARS PEM data), G. Bust (Mid America Computerized Ionospheric Tomography Experiment (MACE) data), C. Ho (GPS TEC data), J. Borovsky and M. Thomsen (LANL particle and field data), L. Cafarella (Istituto Nazionale di Geofisica, Italy, ground magnetometer data). The authors would like to acknowledge use of the 210 Magnetic Meridian (MM) data. The PI, K. Yumoto, manages the 210 MM observations project and group. The database is located at the Solar-Terrestrial Environment Laboratory (STEL) at Nagoya University. The following individuals supported ground magnetic observatories used in this study: K. J. W. Lynn, B. Sukmadradjat, D. Cole, S. Tsunomura, B. J. Fraser ,F. W. Menk, M. Blackford, P. Hattori, J. A. Kennewell , J. K. Chao, S.-W. Chen, R. J. Morris, R. B. Feir, T. Takahasi, E. F. Vershinin, V. V. Bogdaroj, A. V. Buzevich, G. F. Krymsky, V. A. Pilipenko, S. Manurung, O. Sobari, M. Ruhimat, and D. Yeboah-Amankwah.

The editor thanks John Freeman and Roger Smith for their assistance in evaluating this paper.

References

Aarons, J., Global positioning system phase fluctuations at auroral latitudes, *J. Geophys. Res., 102*, 17219, 1997.

Aarons, J., M. Mendillo, and R. Yantosca, GPS phase fluctutations in the equatorial regions during sunspot minimum, *Radio Sci., 32*, 1535, 1997.

Anderson, B. J., J. B. Gary, T. A. Potemra, R. A. Frahm, J. R. Sharber, and J. D. Winningham, UARS observations of Birkeland currents and Joule heating rates for the November 4, 1993, storm, *J. Geophys. Res.*, this issue.

Akasofu, S.-I., Energy coupling between the solar wind and the magnetosphere, *Space Sci. Rev., 28*, 121, 1981.

Baker, D. N., J. B. Blake, D. J. Gorney, and P. R. Higbie, Highly relativistic magnetospheric electrons: A role in coupling to the middle atmosphere?, *Geophys Res Lett., 14*, 1027, 1987.

Baker, D. N., et al., Relativistic electron acceleration and decay time scales in the inner and outer radiation belts: SAMPEX, *Geophys. Res. Lett., 21*, 409, 1994.

Baker, D. N., et al., Recurrent geomagnetic storms and relativistic electron enhancements in the outer magnetosphere: ISTP coordinated measurements, *J. Geophys. Res., 102*, 14155, 1997.

Blanc, M., and A. D. Richmond, The ionospheric disturbance dynamo, *J. Geophys. Res., 85*, 1669, 1980.

Borovsky, J., M. F. Thomsen, and D. J. McComas, The superdense plasma sheet: Plasmaspheric origin, solar wind origin or ionospheric origin?, *J. Geophys. Res., 102*, 22089,1997.

Borovsky, J., M. F. Thomsen, D. J. McComas, T. E. Cayton, and D. J. Knipp, Magnetospheric dynamics and mass flow during the November-1993 storm, *J. Geophys. Res.*, this issue.

Buonsanto, M. J., and T. J. Fuller-Rowell, Strides made in understanding space weather at Earth, *Eos Trans. AGU, 78*, 1, 1997.

Bust, G. S., T. L. Gaussiran II, and D. S. Coco, Ionospheric obser-

vations of the November 1993 storm, *J. Geophys. Res., 102*, 14293, 1997.

Burton, R. K., R. L. McPherron, and C. T. Russell, An empirical relationship between interplanetary conditions and *Dst*, *J. Geophys. Res., 80*, 4204, 1975.

Callis, L. B., et al, Precipitating electrons: Evidence for effects on mesospheric odd nitrogen, *Geophys. Res. Lett., 23*, 1901, 1996a.

Callis, L. B., et al., A 2-D model simulation of downward transport of NO_y into the stratosphere, *Geophys. Res. Lett., 23*, 1905, 1996b.

Chen, J., P. J. Cargill, and P. J. Paladesso, Predicting solar wind structures and geoeffectiveness, *J. Geophys. Res., 102*, 14701, 1997.

Cliver, E. W., V. Boriakoff, and K. Bounar, The 22-year cycle of geomagnetic and solar wind activity, *J. Geophys. Res., 101*, 27091, 1996.

Codrescu, M.V., T. J. Fuller-Rowell, and I. S. Kutiev, Modeling the F layer during specific geomagnetic storms, *J. Geophys. Res., 102*, 14315, 1997a.

Codrescu, M. V., T. J. Fuller-Rowell, R. G. Roble, and D. S. Evans, Medium particle precipitation influences on the mesosphere and lower thermosphere, *J. Geophys. Res., 102*, 19977, 1997b.

Cooper, M. L., C. R. Clauer, B . A Emery, A. D. Richmond, and J. D. Winningham, A storm time assimilative mapping of ionospheric electrodynamics analysis for the severe geomagnetic storm of November 8-9, 1991, *J. Geophys. Res., 100*, 19329, 1995.

Crooker, N. U., and A. H. McAllister, Transients associated with recurrent storms, *J. Geophys. Res., 102*,14041, 1997.

Crooker, N. U., et al., A two-stream, four-sector recurrence pattern: Implications from WIND for the 22-year geomagnetic activity cycle, *Geophys. Res. Lett., 23*, 1275, 1996.

Crowley, G., A. Ridley, D. Winningham, R. Frahm, J. Sharber, and J. Russell, Nitric oxide variations in the mesosphere and lower thermosphere during the November 1993 storm period, *J. Geophys. Res.*, this issue.

Dessler, A. J., and E. N Parker, Hydromagnetic theory of geomagnetic storms, *J. Geophys. Res., 64*, 2239, 1959.

Detrick, D. L., and T. J. Rosenberg, A phased-array radiowave imager for studies of cosmic noise absorption, *Radio Sci., 25*, 325, 1990.

Emery, B. A., et al., Assimilative mapping of ionospheric electrodynamics in thermosphere-ionosphere comparison with global ionospheric and thermospheric observations during GEM SUNDIAL period of March 28-29, 1992, *J. Geophys. Res., 101*, 26681, 1996.

Emery, B. A., et al. , Thermospheric neutral response to the November 1993 sorm, *Eos Trans. AGU, 78*, Fall Meet. Suppl., F520, 1997.

Emery, B. A., C. Lathuillere, P. G. Richards, R. G. Roble, M. Buonsanto, D. J. Knipp, P. Wilkinson, D. Sipler and R. Niciejewski, Thermospheric Neutral Response to the November 1993 Storm, Submitted to *J. Atmos. and Solar Terr. Physics*, 1998.

Engebretson, M., K.-H. Glassmeier, M. Stellmacher, W. J. Hughes, and H. Luhr, The dependence of high latitude Pc 5 wave power on solar wind velocity and the phase of high speed solar wind streams, *J. Geophys. Res*, this issue.

Farley, D. T., E. Bonelli, B. G. Fejer, and M. F. Larsen, The prereversal enhancement of the zonal electric field in the equatorial ionosphere, *J. Geophys. Res., 91*, 13723, 1986.

Feldstein, Y. I., Modeling of the magnetic field of magnetospheric ring current as a function of interplanetary medium parameters, *Space. Sci. Rev., 59*, 83, 1992.

Feldstein , Y. I., and G. V. Starkov, Dynamics of auroral belt and polar geomagnetic disturbances, *Planet. Space Sci., 15*, 209, 1967.

Foster, J. C., and F. J. Rich, Prompt mid-latitude electric field effects during severe geomagnetic storms, *J. Geophys. Res*, this issue.

Foster, J. C., et al., Russian-American Tomography Experiment, *Int. J. Imag. Sys. Tech., 5*, 148, 1994a.

Foster, J. C., et al., Coordinated stable auroral red arc observations: Relationship to plasma convection, *J. Geophys. Res., 99*, 11429, 1994b.

Foster, J. C., S. Cummer, and U. S. Inan, Midlatitude particle and electric field effects at the onset of the November 1993 geomagnetic storm. *J. Geophys. Res*, this issue.

Frahm, R. A., et al., The diffuse aurora: A significant source of ionization in the middle atmosphere, *J. Geophys. Res., 102*, 28203, 1997.

Freeman, J. W., A. Urquhart, and G. Andrews, The November 1993 storm as seen by the Magnetospheric Specification Model, *Eos Trans. AGU, 77*, Spring Meet. Suppl., S235, 1996.

Freeman, J. W., T. P. O'Brien, A. A. Chan, and R. A. Wolf, Energetic electrons at geostationary orbit during the November 3-4 storm: Spatial/temporal morphology, characterization by a power law spectrum, and representation by an artificial neural network, *J. Geophys. Res*, this issue.

Fuller-Rowell, T. J., and D. S. Evans, Height-integrated Pedersen and Hall conductivity patterns inferred from the TIROS-NOAA satellite data, *J. Geophys. Res., 92*, 7606, 1987.

Fuller-Rowell, T. J., M. V. Codrescu, H. Rishbeth, R. J. Moffett, and S. Quegan, On the seasonal response of the thermosphere and ionosphere to geomagnetic storms, *J. Geophys. Res., 101*, 2343, 1996.

Fuller-Rowell, T. J., M. V. Codrescu, R. G. Roble, and A. D. Richmond, How does the thermosphere and ionosphere react to a geomagnetic storm?, in *Magnetic Storms, Geophys. Monogr. Ser., vol 98*, edited by B. T. Tsurutani, W. D. Gonzalez, Y. Kamide and J. K. Araballo, p. *203*, AGU, Washington, D. C., 1997.

Gonzalez, W. D., and B. T. Tsurutani, Criteria of interplanetary parameters causing intense magnetic storms (*Dst* < -100nT), *Planet. Space Sci.*, 35, 1101, 1987.

Gonzalez, W. D., et al., What is a geomagnetic storm?, *J. Geophys. Res., 99*, 5771, 1994.

Gosling, J. T., G. Borrini, J. R. Asbridge, S. J. Bame, W. C. Feldman, and R. T. Hansen, Coronal streamers in the solar wind at 1 AU, *J. Geophys. Res., 86*, 5438, 1981.

Gussenhoven, M. S., D. A. Hardy, and N. Heinemann, Systematics of the equatorward diffuse auroral boundary, *J. Geophys. Res., 88*, 5692, 1983.

Gussenhoven, M. S., E. G. Mullen, R. C. Filz, D. H. Brautigam and F. A. Hanser, New low-altitude does measurements, *IEEE Trans. Nuc. Sci., 34*, 676, 1987.

Hairston, M. R., R. A. Heelis, and F. J. Rich, Analysis of the ionospheric cross polar cap potential drop using DMSP data during the National Space Weather Program study period, *J. Geophys. Res.*, this issue.

Heelis, R. A., P. C. Kendall, R. J. Moffett, D. W. Windle, and H. Rishbeth, Electrical coupling of the E and F-regions and its effect on F-region drifts and winds, *Planet. Space Sci., 22*, 743, 1974.

Ho, C. M., et al., Ionospheric total electron content perturbations monitored by GPS during two northern hemisphere winter storms in solar declining phase, *J. Geophys. Res.*, this issue.

Hoogeveen G. W., and A. R. Jacobson, Radio interferometer measurements of plasmasphere density structures during geomagnetic storms, *J. Geophys. Res., 102*, 14177, 1997.

Joselyn, J. A., Geomagnetic activity forecasting: State of the art, *Rev. Geophys., 33*, 383, 1995.

Kelley, M. C., *The Earth's Ionosphere, Plasma Physics and Electrodynamics*, Academic Press, 1989.

Kim, H.-J., and A. A. Chan, Fully adiabatic changes in storm time relativistic electron *J. Geophys. Res., 102*, 22107,1997.

Knipp, D. J., and B. A. Emery, A report on the geomagnetic study of the early November 1993 geomagnetic storm, *Adv. Space Res., 22*, 41, 1998.

Knipp, D. J., and B. A. Emery, Mapping ionospheric substorm response, *Adv. Space Res., 20*, 895,1997.

Kokubun, S., L. et al., Large field events in the distant magnetotail during magnetic storms, *J. Geomagn. Geoelectr., 48*, 561, 1996.

Korth, A., and R. H. W. Friedel, Dynamics of energetic ions and electrons between L=2.5 and L=7 during magnetic storms. *J. Geophys. Res., 102*, 14113, 1997.

Kozyra, J. U., et al., Effects of a high density plasma sheet on ring current development during the November 2-6, 1993, magnetic storm, *J. Geophys. Res.*, this issue.

Kozyra, J. U., V. K. Jordanova, R. B. Horne, and R. M., Modeling of the contributions of electromagnetic ion cyclotron (EMIC) waves to stormtime ring current erosion, in *Magnetic Storms, Geophys. Monogr. Ser.*, vol. 98, edited by B. T. Tsurutani, W. D.

Gonzalez, Y. Kamide, and J. K. Araballo, p. 187, AGU, Washington, D. C., 1997.

Li, X., et al., Multi-satellite observations of the outer zone electron variation during the 3-4 November 1993 geomagnetic storm, *J. Geophys. Res., 102*, 14123, 1997.

Lu, G., A. D. Richmond, B. A. Emery, R. G. Roble, Magnetosphere-Ionosphere-Thermosphere Coupling; Effect on neutral winds on Joule Heating and Field Aligned Currents, *J. Geophys. Res., 100*, 19643, 1995.

Lu, G., et al., High-latitude ionospheric electrodynamics as determined by assimilative mapping of ionospheric electrodynamics procedure for the conjugate SUNDIAL/ATLAS1/GEM period of March 28-29, 1992, *J. Geophys. Res., 101*, 26697, 1996.

Lu G., et al., Global energy deposition during the January 1997 magnetic cloud event, *J. Geophys. Res., 103*, 11685, 1998.

Lui, A. T. Y., D. J. Williams, R. W. McEntire, S. P. Christon, A. B. Gavin, and D. J. Knipp, Energetic ion composition and charge state of solar wind plasma during the November 3, 1993, magnetic storm, *J. Geophys. Res.*, this issue.

Maruyama, T., and N. Matuura, Longitudinal variability of annual changes in activity of equatorial spread F and plasma bubbles, *J. Geophys. Res., 89*, 10903, 1984.

McAllister, A. H., and N. U. Crooker, Coronal mass ejections, corotating interaction regions and geomagnetic storms, in *Coronal Mass Ejections: Causes and Consequences, Geophys. Monogr. Ser.*, vol 99, edited by N. Crooker, J. Joselyn and J. Feynman, p. 279, AGU, Washington, D. C., 1997.

McAllister, A. H., D. Knipp, N. U Crooker, T. Mukai, and S. Kokubun, Identification of solar drivers: The 3-4 November 1993 geomagnetic storm, *J. Geophys. Res.*, this issue.

McHarg, M. G., J. V. Olson, and P. T. Newell, ULF cusp pulsations: Diurnal variations and interplanetary magnetic field correlations with ground-based observations, *J. Geophys. Res., 100*, 19729, 1995.

McPherron, R. L., Magnetospheric dynamics, in *Introduction to Space Physics*, edited by M. G. Kivelson and C. T. Russell, p. 412, Cambridge Univ. Press, New York, 1995.

Mendillo, M., J. Baumgardner, X. Pi, P. J. Sultanand, and R. Tsunoda, Onset conditions for equatorial spread *F*, *J. Geophys. Res., 97*, 13865, 1992.

Mursula, K., and B. Zieger, The 13.5-day periodicity in the Sun, solar wind, and geomagnetic activity: The last three solar cycles, *J. Geophys. Res., 101*, 27077, 1996.

Mursula, K., T. Braysy, and G. Marklund, ULF wave activity above the ionosphere during magnetic storms, Paper presented at the 31st Scientific Assembly of COSPAR, p. 216, 1996.

Nakamura, R., D. N. Baker, J. B. Blake, S. Kanekal, B. Klecker, and D. Hovestadt, Relativistic electron precipitation enhancements near the outer edge of the radiation belt. *Geophys. Res Lett., 22*, 1129, 1995.

Nakamura, R., S. Kokubun, T. Mukai, and T. Yamamoto, Changes in the distant tail configuration during geomagnetic storms, *J. Geophys. Res., 1021*, 9587, 1997.

Nakamura, R., K. Kamei, Y. Kamide, D. N. Baker, J. B. Blake, and M. Looper, SAMPEX observations of storm-associated electron flux variations in the outer radiation belt, *J. Geophys. Res.*, this issue.

Paulikas, G. A., and J. B. Blake, Effects of the solar wind on magnetospheric dynamics: Energetic electrons at the synchronous orbit, in *Quantitative Modeling of Magnetospheric Processes, Geophys. Monogr. Ser.*, vol. 21, edited by W. P. Olsen, p. 180, AGU, Washington, D. C., 1979.

Pi, X., A. J. Mannucci, U. J. Lindqwister,and C. M. Ho, Monitoring of global ionospheric irregularities using the worldwide GPS network, *Geophys. Res. Lett., 24*, 2283, 1997.

Prölss, G., Magnetic storm associated perturbations of the upper atmosphere, in *Magnetic Storms, Geophys. Monogr. Ser.*, vol. 98, edited by B. T. Tsurutani, W. D. Gonzalez, Y. Kamide, and J. K. Araballo, p. 227, AGU, Washington, D. C., 1997.

Reeves, G. D., Relativistic electrons and magnetic storms: 1992-1995, *J. Geophys. Res.* in press, 1998.

Richards, R. G., and P. J. Wilkinson, The ionosphere and thermosphere at southern midlatitudes during the November 1993 ionospheric storm: A comparison of measurement and modeling, *J. Geophys. Res., 103*, 9373. 1998.

Richmond, A. D., Assimilative mapping of ionospheric electrodynamics, *Adv. Space Sci.*, (6), 69, 1992.

Richmond, A. D., and Y. Kamide, Mapping electrodynamic features of the high-latitude ionosphere from localized observation: Technique, *J. Geophys. Res., 93*, 5741, 1988.

Richmond, A. D., G. Lu, B. A. Emery, and D. J. Knipp, The AMIE procedure: Prospects for space weather specification and prediction, *Adv. Space Res, 22*, 103, 1998.

Ridley, A. C., T. Moretto, P. Ernstrom, and C. R. Clauer, Global analysis of three traveling convection vortex events during the November 1993 storm using the assimilative mapping of ionospheric electrodynamics technique, *J. Geophys. Res.*, this issue.

Rosenberg, R. L., and P. J. Coleman Jr., Heliographic latitude dependence of the dominant polarity of the interplanetary magnetic field, *J. Geophys. Res., 74*, 5611, 1969.

Rostoker, G., S.-I. Akasofu, J. Foster, R. A. Greenwald, Y. Kamide, K. Kawasaki, A T. Y. Lui, R. L. McPherron, and C. T. Russell, Magnetospheric substorms-definitions and signatures, *J. Geophys. Res., 85*, 1663, 1980.

Rostoker, G., Correlated measurements of relativistic electrons at SAMPEX with ULF measurements from the CANOPUS magnetometer chain, Paper presented at IUGG XII General Assembly, Boulder, Colo., 1995.

Russell, C. T., and R. M Thorne, On the structure of the inner magnetosphere, *Cosmic, Electrodyn., 1*, 67, 1970

Russell, C. T., and R. L. McPherron, Semiannual variation of geomagnetic activity, *J. Geophys. Res. 78*, 92, 1973.

Sharber, J. R., et al., UARS particle environment monitor observations during the November 1993 storm: Auroral morphology, spectral characterization, and energy deposition, *J. Geophys. Res.*, this issue.

Shiokawa, K., C.-I. Meng, G. D. Reeves, F. J. Rich, and K. Yumoto, A multi-event study of broadband electrons observed by the DMSP satellites and their relation to red aurora observed at mid-latitude stations, *J. Geophys. Res.*, 102, 14237, 1997.

Siscoe, G., ISM results: Global geometry of magnetopause reconnection for the IMF By, paper presented at NSF GEM '97 Summer Workshop, Snowmass, Colo., 1997.

Slinker, S. P., J. A. Fedder, J. Chen, and J. G. Lyon, Global MHD simulation of the magnetosphere and ionosphere for 1930-2330 UT on 3 November 1993, *J. Geophys. Res.*, this issue.

Stauning, P., T. Moretto, E. Friis-Christensen, and O. Rasmussen, The space weather event of 3-5 November, 1993, *Tech. Rep., 95-15*, Danish Meteorol. Inst., Copenhagen, Denmark, 1995.

Stauning, P., Substorm modeling based on observations of an intense high-latitude absorption surge event. *J. Geophys. Res.*, this issue.

Thorne, R. M., Energetic radiation belt precipitation: A natural depletion mechanism for stratospheric ozone, *Science, 21*, 287, 1977.

Troshichev, O. A., V. G. Andrezen, S. Vennerstrøm, and E. Friis-Christensen, Magnetic activity in the polar cap - A new index, *Planet. Space Sci.*, 1095, 1988.

Troshichev, O. A., H. Hayakawa, A. Mutsuoka, T. Mukai, and K Tsuruda, Cross polar cap diameter and voltage as a function of PC index and interplanetary quantities, *J. Geophys. Res.*, 101, 13429, 1996.

Tsurutani, B. T., and W. D. Gonzalez, The cause of high-intensity long-duration continuous AE activity (HILDCAA's): Interplanetary Alfven wave trains, *Planet. Space Sci., 35*, 405, 1987.

Tsurutani, B. T., W. D. Gonzalez, A. L. C. Gonzalez, F. Tung, J. K. Arbollo, and M. Okada, Interplanetary origin of geomagnetic activity in the declining phase of the solar cycle, *J. Geophys. Res.,. 100*, 21717, 1995.

Vennerstrøm, S. V., E. Friis-Christensen, O. A. Troshichev, and V. G. Andresen, Comparison between the polar cap index, PC and the auroral electrojet indices, *AE, AL* and *AU, J. Geophys. Res. 96*, 101, 1991.

Watari, S., Soft X-ray coronal holes and interplanetary disturbances, paper presented at IUGG XXI General Assembly, Boulder, Colo., 1995.

Weatherwax,. A. T., T. J. Rosenburg, C. G. MacClennan, and J. H. Dolittle, Substorm precipitation in the polar cap and associated Pc 5 modulation, *Geophys. Res. Lett., 24*, 579, 1997.

Williams, D. J., A 27-day periodicity in outer zone trapped electron intensities, *J. Geophys. Res., 71*, 1815, 1966.

Weimer, D. R., Models of high-latitude electric potentials derived with a least squares error fit of spherical harmonic coefficients, *J. Geophys. Res.*, *100*, 19595, 1995.

Winterhalter, D., E. J. Smith, M. E. Burton, N. Murphy, and D. J. McComas, The heliospheric plasmasheet, *J. Geophys. Res.*, *99*, 6667, 1994.

Yokoyama, N., and Y. Kamide, Statistical nature of geomagnetic storms, *J. Geophys. Res.*, *102*, 14215, 1997.

Zesta, E. W., J. Hughes, and M. J. Engebretson, The evolution of traveling convection vortices (TCVs) *Eos Trans. AGU, 76*, Fall Meet. Suppl., F516, 1995.

F. Chun, D. J. Knipp, M. G. McHarg, and K. Mosely, Department of Physics, U.S. Air Force Academy, USAF Academy, CO 80840 (email: chunfk.dfp@usafa.af.mil; knippdj.dfp@usafa.af.mil; mchargmg.dfp@usafa.af.mil)

M. Codrescu and D. Evans, Space Environment Center, National Oceanic and Atmospheric Research, Boulder, CO 80303. (email: codrescu@sec.noaa.gov)

B. A. Emery and A. H. McAllister, High Altitude Observatory, National Center for Atmospheric Research, Boulder, CO 80307. (email: emery@ncar.ucar.edu; ahm@ncar.ucar.edu)

M. Engebretson, Department of Physics, Augsburg College, Minneapolis, MN 55454. (email: engebret@augsburg.edu)

S. Kokubun, Solar Terrestrial Environment Laboratory, Nagoya University, 3-13 Honohara Toyokawa, Aichi 442, Japan.

L. Lanzerotti, Bell Laboratories, Lucent Technology, 600 Mountain Avenue, Murray Hill, NJ 07974. (email: ljl@physics.bell-labs.com)

X. Li, Laboratory for Atmospheric and Space Physics, University of Colorado, Boulder, CO 80303. (email: lix@kitron.Colorado.edu)

T. Mukai, Institute for Space and Astronautical Science, 3-1-1 Yoshinodai Sagamihara, Kanagawa 229, Japan. (email: mukai@fujitubo.gtl.isas.ac.jp)

T. Obara, Hiraiso Solar Terrestrial Research Center, Ibaraki, Japan. (email: T.Obara@crl.go.jp)

X. Pi, Jet Propulsion Laboratory, California Institute of Technology, 4800 Oak Grove Drive, Pasadena, CA. (email: xqp@cobra.jpl.nasa.gov)

G. D. Reeves, Los Alamos National Laboratory, Los Alamos, NM 87545. (email: reeves@lanl.gov)

F. J. Rich, Space Vehicles Directorate, Air Force Research Laboratory, Hanscom Air Force Base, MA 01731. (email: rich@plh.af.mil)

T. Rosenberg and A. Weatherwax, Institute for Physical Science and Technology, University of Maryland at College Park, College Park, MD 20742-2431. (email: rosenberg@uap.umd.edu: allanw@polar.umd.edu)

J. Sharber, Southwest Research Institute, San Antonio, TX 78228. (email: sharb@broccoli.spacc.swri.edu)

P. Wilkinson, IPS Radio and Space Services, Haymarket, New South Wales, Australia. (email: phil@ips.gov.au)

(Received December 9, 1997; revised February 24, 1998; accepted February 27, 1998.)